

Effect Decomposition of Functional-Output Computer Experiments via Orthogonal Additive Gaussian Processes

Yu Tan, Yongxiang Li*

Department of Industrial Engineering and Management,
Shanghai Jiao Tong University

Xiaowu Dai

Department of Statistics and Data Science and Department of Biostatistics,
University of California at Los Angeles

Kwok-Leung Tsui

Department of Industrial, Manufacturing, and Systems Engineering,
The University of Texas at Arlington

Abstract

Functional ANOVA (FANOVA) is a widely used variance-based sensitivity analysis tool. However, studies on functional-output FANOVA remain relatively scarce, especially for black-box computer experiments, which often involve complex and nonlinear functional-output relationships with unknown data distribution. Conventional approaches often rely on predefined basis functions or parametric structures that lack the flexibility to capture complex nonlinear relationships. Additionally, strong assumptions about the underlying data distributions further limit their ability to achieve a data-driven orthogonal effect decomposition. To address these challenges, this study proposes a functional-output orthogonal additive Gaussian process (FOAGP) to efficiently perform the data-driven orthogonal effect decomposition. By

*Contact: Yongxiang Li, yongxiangli@sjtu.edu.cn, Department of Industrial Engineering and Management, Shanghai Jiao Tong University, Shanghai 200240.

enforcing a conditional orthogonality constraint on the separable prior process, the proposed functional-output orthogonal additive kernel enables data-driven orthogonality without requiring prior distributional assumptions. The FOAGP framework also provides analytical formulations for local Sobol’ indices and expected conditional variance sensitivity indices, enabling comprehensive sensitivity analysis by capturing both global and local effect significance. Validation through two simulation studies and a real case study on fuselage shape control confirms the model’s effectiveness in orthogonal effect decomposition and variance decomposition, demonstrating its practical value in engineering applications.

Keywords: Computer experiments; Surrogate modeling; Kriging; Functional-output FANOVA; Effect decomposition.

1 Introduction

Functional ANOVA (FANOVA, Efron and Stein 1981; Sobol’ 2001) has become one of the most popular variance-based sensitivity analyses (Zhang et al., 2024), widely applied in ischemic heart screening (Zhang et al., 2019), additive manufacturing (Centofanti et al., 2023) and automated machine learning hyper-parameters tuning (Garouani and Bouneffa, 2024). By decomposing the output variance and quantifying the importance of input variables through using Sobol’ indices (Sobol’, 1990, 1993), FANOVA serves as a critical tool for variable importance selection (Fang et al., 2005; Santner et al., 2018), dimensionality reduction (Muehlenstaedt et al., 2012; Sung et al., 2020; Lu et al., 2022), and improving model interpretability (Chen et al., 2023).

Despite extensive research on FANOVA (Muehlenstaedt et al., 2012; Janon et al., 2014; Ginsbourger et al., 2016; Liu et al., 2021; Centofanti et al., 2023; Marnissi and Leiber, 2024), studies on functional-output FANOVA (FOFANOVA) remain relatively scarce, especially in the context of computer experiments with black-box functional outputs (responses), where physical experiments are prohibitively expensive or computer simulations are time-consuming (Kokoszka and Reimherr, 2017). Within the FOFANOVA framework, we study both effect decomposition and variance decomposition in this study because effect decompo-

sition is as critical as variance decomposition, with the two being inherently interconnected and complementary. Specifically, effect decomposition establishes the theoretical foundation for variance decomposition (Durrande et al., 2013; Xiao et al., 2018; Zhang et al., 2024), while variance decomposition serves as a practical tool to quantify the significance of the effects and their corresponding input variables (Hooker, 2004; Muehlenstaedt et al., 2012; Sung et al., 2020; Apley and Zhu, 2020). Moreover, effect decomposition provides insights into input-output relationships in black-box computer experiments, thereby improving model interpretability (Duvenaud et al., 2011; Durrande et al., 2012; Sung et al., 2020).

The first step in applying FOFANOVA to computer experiments is functional-output surrogate modeling. The general functional-output regression model dates back to Faraway (1997), which is a linear and parametric regression approach. To exploit spatial-temporal correlation in computer experiments with functional outputs, Shi et al. (2007) proposed a nonlinear and nonparametric approach, called Gaussian process (GP) functional regression. Rougier (2008) tackled the challenge of high-dimensional functional outputs by utilizing a separable covariance structure, enabling efficient emulation of functional outputs. To further enhance scalability, Wang et al. (2021) proposed a multi-fidelity high-order GP by leveraging basis decomposition to reduce model parameters, which captures complex correlations between outputs and integrates multi-fidelity. Ma et al. (2022) employed nearest-neighbor GP with built-in input dimensionality reduction via active subspaces, which significantly reduced the dimensionality of both input and output spaces. To adequately capture output spatial correlations, Liu et al. (2024) proposed a novel one-stage method called latent functional GP.

The primary application of FOFANOVA is to identify important input variables through variance decomposition. To assess the importance of each input on the time-series output, Drignei (2010) applied FANOVA at each time point and averaged the FANOVA results to obtain the expected conditional variance (ECV) sensitivity indices. Shi et al. (2018) ex-

tended FANOVA by incorporating temporal covariance and applying covariance decomposition to derive a global dynamic sensitivity index, which measures the variable importance at different time points. It has been shown that while many computer experiments have complex functional outputs, these functional outputs are often driven by a relatively small subset of important input variables (Drignei, 2010; Wagener and Pianosi, 2019; Jiang et al., 2021; Chiogna et al., 2024).

Although these methods perform well in variance decomposition within FOFANOVA, relatively little attention has been paid to the effect decomposition of functional outputs or functional-output effect decomposition (FOED). Existing methods (Cheng and Lu, 2019; Yue et al., 2019; Bolin et al., 2021) for FOED largely rely on linear or parametric functional regression, and the use of predefined (user-specified) basis functions imposes additional assumptions on the underlying data distribution for orthogonality, such as uniformity. In addition, the lack of data-driven orthogonality can lead to incorrect attributions of variable/effect importance, as demonstrated in the case of scalar outputs (Durrande et al., 2012; Lu et al., 2022). These limitations can lead to biased or inaccurate regression for datasets from black-box computer experiments, which often involve complex and nonlinear relationships with unknown data distribution (Santner et al., 2018). The nonlinearity and the unknown data distribution in functional-output computer experiments (Hooker, 2007; Rao and Reimherr, 2023; Centofanti et al., 2023) pose significant challenges for FOFANOVA.

To address the aforementioned issues, this study proposes a data-driven methodology for efficient FOED, which is referred to as functional-output orthogonal additive Gaussian process (FOAGP). Initially, functional outputs are modeled by a sum of several effects, including high-order effects. To enforce orthogonality on the underlying data distribution, the functional-output orthogonal additive kernel is proposed, which enables data-driven orthogonality and transforms each effect into an orthogonal one. By incorporating the proposed kernel into the AGP framework, a nonlinear and nonparametric FOAGP model is proposed for FOED. Furthermore, the design of the proposed kernel utilizes the Hadamard

product to ensure that the computational complexity of the FOAGP modeling remains comparable to the standard GP modeling. We then prove that the FOED based on the proposed FOAGP model is exactly the orthogonal decomposition.

Based on the proposed FOED, the corresponding variance decomposition is further established for sensitivity analysis. Within the FOAGP framework, we derive analytical local Sobol’ indices for local sensitivity analysis, which capture the local effect significance at each output position. Additionally, we derive analytical ECV sensitivity indices for global sensitivity analysis, which measure the whole contribution of effects over the whole output space. For practical purposes, the corresponding estimators for both sensitivity analyses are provided. It is worth noting that all the estimators for the sensitivity analysis rely solely on the training dataset, enabling global local sensitivity analysis without prior knowledge about the underlying data distribution. The proposed FOED and global local sensitivity analysis make the proposed FOAGP model a unified data-driven implementation of FOFANOVA.

The remainder of the paper is organized as follows. Sec. 2 provides a brief review of FANOVA for computer experiments with scalar and time-series outputs and orthogonal additive GP (OAGP). Sec. 3 introduces the proposed FOAGP framework, covering the modeling, FOED, and global local variance decomposition. Sec. 4 provides simulation examples to demonstrate the effectiveness of FOAGP. A real case study on fuselage shape control in Sec. 5 further validates the the applicability and effectiveness of FOAGP. Finally, Sec. 6 concludes the paper and outlines possible directions for future research. All the proofs of the theorems in this study can be found in the appendix.

2 Review of Previous Work

This section begins with a brief review of FANOVA for computer experiments with scalar and time-series outputs, followed by a discussion of the time-variant high dimensional model

representation. It then provides a summary of OAGP and its connection to FANOVA.

2.1 FANOVA

FANOVA is a sophisticated tool for global sensitivity analysis in computer experiments, allowing analysts to decompose the output of a computer model into its fundamental effects and quantify the significance of each effect (Owen, 2014). Let $f : \mathbb{R}^d \rightarrow \mathbb{R}$ be a square-integrable function of $\mathbf{x} = (x_i)_{i \in \mathcal{D}}$ and the components $\{x_i\}_{i \in \mathcal{D}}$ are assumed to be independent, where $\mathcal{D} = \{1, \dots, d\}$. The FANOVA decomposition (Sobol', 1990; Owen and Prieur, 2017) of $f(\mathbf{x})$ is defined as

$$f(\mathbf{x}) = f_0 + f_1(x_1) + f_2(x_2) + \dots + f_{12}(x_1, x_2) + \dots + f_{12\dots d}(x_1, \dots, x_d) = \sum_{\mathbf{u} \subseteq \mathcal{D}} f_{\mathbf{u}}(\mathbf{x}_{\mathbf{u}}), \quad (1)$$

where $f_{\mathbf{u}}(\mathbf{x}_{\mathbf{u}})$ is a function of $\mathbf{x}_{\mathbf{u}} = (x_i)_{i \in \mathbf{u}}$ corresponding to a subset \mathbf{u} of \mathcal{D} , and is referred to as the effect function or effect for simplicity. When $\mathbf{u} = \emptyset$, the effect function f_{\emptyset} degenerates to a constant and is denoted as f_0 . The constant effect f_0 is defined as the expectation of $f(\mathbf{x})$, denoted as $\mathbb{E}_{\mathbf{x}}[f(\mathbf{x})]$, and the remaining effects $\{f_{\mathbf{u}}\}_{\mathbf{u} \neq \emptyset}$ are determined by the orthogonality constraints

$$\int f_{\mathbf{u}}(\mathbf{x}_{\mathbf{u}}) dF_i(x_i) = 0 \quad (\forall i \in \mathbf{u}), \quad (2)$$

where $F_i(x_i)$ is the cumulative distribution function (CDF) of the i th component x_i . Due to the orthogonality between the effects $\{f_{\mathbf{u}}\}$, the FANOVA decomposition in Eq. (1) is also referred to as orthogonal effect decomposition.

The variance decomposition of FANOVA directly follows the orthogonal effect decomposition:

$$\mathbb{V}_{\mathbf{x}}(f(\mathbf{x})) = \sum_{\mathbf{u} \subseteq \mathcal{D}} \mathbb{V}_{\mathbf{x}_{\mathbf{u}}}(f_{\mathbf{u}}(\mathbf{x}_{\mathbf{u}})),$$

where $\mathbb{V}_{\mathbf{x}}(f(\mathbf{x}))$ denotes the variance of $f(\mathbf{x})$, i.e., $\mathbb{V}_{\mathbf{x}}(f(\mathbf{x})) = \mathbb{E}_{\mathbf{x}}[(f(\mathbf{x}) - \mathbb{E}_{\mathbf{x}}[f(\mathbf{x})])^2]$. Based on the variance decomposition, the relative importance of component subsets $\{\mathbf{u}\}_{\mathbf{u} \subseteq \mathcal{D}}$ can be quantified by Sobol' indices (Sobol', 1990, 1993), which is defined as

$$\phi_{\mathbf{u}} = \frac{\mathbb{V}_{\mathbf{x}_{\mathbf{u}}}(f_{\mathbf{u}}(\mathbf{x}_{\mathbf{u}}))}{\mathbb{V}_{\mathbf{x}}(f(\mathbf{x}))} = \frac{\mathbb{V}_{\mathbf{x}_{\mathbf{u}}}(f_{\mathbf{u}}(\mathbf{x}_{\mathbf{u}}))}{\sum_{\mathbf{v} \subseteq \mathcal{D}} \mathbb{V}_{\mathbf{x}_{\mathbf{v}}}(f_{\mathbf{v}}(\mathbf{x}_{\mathbf{v}}))}. \quad (3)$$

To address the variance dominance of t in time series and assess the importance of each input on the time-series outputs, Drignei (2010) theoretically applied FANOVA at any fixed time point to obtain the time-conditional orthogonal effect decomposition $f(\mathbf{x}, t) = \sum_{\mathbf{u} \subseteq \mathcal{D}} f_{\mathbf{u}|t}(\mathbf{x}_{\mathbf{u}}, t)$ and took the expectation of time-conditional variance with respect to time t to derive the ECV decomposition $\mathbb{E}_t[\mathbb{V}_{\mathbf{x}}(f(\mathbf{x}, t))] = \sum_{\mathbf{u} \subseteq \mathcal{D}} \mathbb{E}_t[\mathbb{V}_{\mathbf{x}_{\mathbf{u}}}(f_{\mathbf{u}|t}(\mathbf{x}_{\mathbf{u}}, t))]$. Normalizing the ECV $\mathbb{E}_t[\mathbb{V}_{\mathbf{x}_{\mathbf{u}}}(f_{\mathbf{u}|t}(\mathbf{x}_{\mathbf{u}}, t))]$ yielded the ECV sensitivity indices

$$\mathcal{S}_{\mathbf{u}} = \frac{\mathbb{E}_t[\mathbb{V}_{\mathbf{x}_{\mathbf{u}}}(f_{\mathbf{u}|t}(\mathbf{x}_{\mathbf{u}}, t))]}{\sum_{\mathbf{v} \subseteq \mathcal{D}} \mathbb{E}_t[\mathbb{V}_{\mathbf{x}_{\mathbf{v}}}(f_{\mathbf{v}|t}(\mathbf{x}_{\mathbf{v}}, t))]} \quad (4)$$

To circumvent the time-conditional orthogonal effect decomposition of time-series outputs, Drignei (2010) employed the standard orthogonal effect decomposition incorporating t as an additional variable to calculate the ECV sensitivity indices through

$$\mathcal{S}_{\mathbf{u}} = \phi_{\mathbf{u}} + \phi_{\mathbf{u}, t}, \quad (5)$$

where numerical integration techniques were used.

Cheng and Lu (2019) introduced the time-variant high dimensional model representation (HDMR) $f(\mathbf{x}, t) \approx \sum_{|\mathbf{u}| \leq 2} f_{\mathbf{u}|t}(\mathbf{x}_{\mathbf{u}}, t)$, where $|\mathbf{u}|$ is the cardinality of the set \mathbf{u} , and further approximated the effect functions using a set of orthogonal polynomials, yielding

$$\begin{aligned}
f(\mathbf{x}, t) \approx & \sum_{i=1}^o \alpha_i \varphi_i(t) + \sum_{i=1}^d \sum_{p+q \leq o} \beta_{pq}^{(i)} \varphi_p(x_i) \varphi_q(t) \\
& + \sum_{1 \leq i < j \leq d} \sum_{p+q+r \leq o} \gamma_{pqr}^{(ij)} \varphi_p(x_i) \varphi_q(x_j) \varphi_r(t), \tag{6}
\end{aligned}$$

where $\{\varphi_p(\cdot)\}_{p=1,2,\dots}$ denoted the orthogonal polynomials basis functions of order p , $\{\alpha_i, \beta_{pq}^{(i)}, \gamma_{pqr}^{(ij)}\}$ represented the basis function coefficients and o was the truncated order of the polynomial basis functions. The coefficients $\{\alpha_i, \beta_{pq}^{(i)}, \gamma_{pqr}^{(ij)}\}$ can be estimated within a Gaussian process framework (Cheng and Lu, 2019). For simplicity, we will refer to the truncated HDMR model in Eq. (6) as the HDMR model throughout the rest of the study.

When the input variable x_i follows a uniform distribution on a specified interval, which is determined by the predefined orthogonal basis functions, the HDMR model in Eq. (6) performs the two-way orthogonal effect decomposition, provided the truncated order is sufficiently large. However, this reliance on a uniform distribution introduces a significant limitation in the black-box computer experiments with functional outputs, where prior knowledge about the underlying data distribution is often unavailable. Consequently, the orthogonality assumed by the HDMR model may not hold in practice. Moreover, the parametric structure and truncated order limits the number of basis functions, restricting regression flexibility of the HDMR model. This limitation may lead to biased or inaccurate predictions (Sung et al., 2020), especially when the high-order effects are present in the experiments.

2.2 Orthogonal Additive Gaussian Processes

Duvenaud et al. (2011) proposed AGP by incorporating an additive structure within GP

$$f(\mathbf{x}) = f_1(x_1) + f_2(x_2) + \dots + f_{12}(x_1, x_2) + \dots + f_{12\dots d}(x_1, \dots, x_d) = \sum_{\mathbf{u} \subseteq \mathcal{D}} f_{\mathbf{u}}(\mathbf{x}_{\mathbf{u}}), \tag{7}$$

where each effect function $f_{\mathbf{u}}(\mathbf{x}_{\mathbf{u}})$ is also a GP. This additive structure is the same as that of orthogonal effect decomposition in Eq. (1), except for the absence of the constant effect f_0 . In practice, the additive structure is enforced through the use of an additive kernel. Given the kernel $k_i(\cdot)$ associated with the i th input x_i , the n th-order additive kernel (Duvenaud et al., 2011) is defined as

$$k_{add_n}(\mathbf{x}, \mathbf{x}') = \lambda_n^2 \sum_{|\mathbf{u}|=n} \prod_{i \in \mathbf{u}} k_i(x_i, x'_i) \quad (8)$$

for $1 \leq n \leq d$, where λ_n^2 is the n th-order variance, and x_i, x'_i are the i th components of \mathbf{x}, \mathbf{x}' , respectively.

Lu et al. (2022) proposed OAGP by applying the orthogonality constraints in Eq. (2) on effect functions $\{f_{\mathbf{u}}(\mathbf{x}_{\mathbf{u}})\}$ in Eq. (7), resulting in an orthogonal additive kernel for each effect function. To capture the mean and ensure identifiability, the constant mean effect f_0 is also included. Using this construction, Lu et al. (2022) demonstrated that OAGP performs exact orthogonal effect decomposition of scalar outputs, and deduced the analytical formulas of Sobol' indices for practical variance decomposition.

3 Functional-Output Orthogonal Additive Gaussian Process

This section details the proposed FOAGP framework, beginning with a description of its additive structure in Sec. 3.1, followed by the proposed functional-output orthogonal additive kernel in Sec. 3.2. The parameter estimation of FOAGP is provided in Sec. 3.3. Sec. 3.4 reveals that the proposed FOAGP model performs exactly orthogonal decomposition. Finally, Sec. 3.5 details the global local variance decomposition within FOAGP framework and provides analytical local Sobol' indices and analytical ECV sensitivity indices, enabling comprehensive sensitivity analysis.

3.1 Model Formulation of FOAGP

In this study, we only consider one-dimensional functional output case for simplicity. In fact, many computer experiments, such as the fuselage shape control Liu et al. (2024), only have one-dimensional functional outputs.

Denote the response of the input \mathbf{x} at the output position t by

$$y(\mathbf{x}, t) = f(\mathbf{x}, t) + \epsilon, \quad (9)$$

where $f(\mathbf{x}, t)$ follows an AGP, and $\epsilon \sim \mathcal{N}(0, \sigma^2 \delta_0^2)$ represents the independent and identically distributed measurement errors that are independent of $f(\mathbf{x}, t)$. In this study, we assume that the proposed model has the following additive structure

$$\begin{aligned} f(\mathbf{x}, t) &= \sum_{\mathbf{u} \subseteq \mathcal{D}} f_{\mathbf{u}|t}(\mathbf{x}_{\mathbf{u}}, t) \\ &= f_{0|t}(t) + f_{1|t}(x_1, t) + \cdots + f_{12|t}(x_1, x_2, t) + \cdots + f_{1\dots d|t}(x_1, \dots, x_d, t), \end{aligned} \quad (10)$$

where each functional-output effect function $f_{\mathbf{u}|t}(\mathbf{x}_{\mathbf{u}}, t)$ also follows a GP with zero mean. For simplicity, $f_{\mathbf{u}|t}(\mathbf{x}_{\mathbf{u}}, t)$ will be referred to as the functional-output effect or simply the effect throughout this study. The decomposition of $f(\mathbf{x}, t)$ in Eq. (10) is called FOED.

Unlike the OAGP model with a global constant mean effect (Lu et al., 2022), the proposed model includes a mean effect $f_{0|t}(t)$ that depends on the output position t and is determined by a conventional kernel $k_t(\cdot)$ without orthogonality constraints (Durrande et al., 2012). This mean effect $f_{0|t}(t)$ extracts the mean of the functional output $y(\mathbf{x}, t)$ at any output position, enabling other effects $\{f_{\mathbf{u}|t}(\mathbf{x}_{\mathbf{u}}, t) \mid \mathbf{u} \neq \emptyset\}$ to have zero mean. Without this mean effect $f_{0|t}(t)$, the model may have identifiability issues because any constant could be added to one effect and subtracted from another.

Instead of directly applying the traditional FANOVA decomposition as in Eq. (1) by treating the output position t as an additional variable, the proposed model focuses on

the effect decomposition with respect to the input \mathbf{x} . One key reason for this is that the variance dominance of t can obscure the importance of input variables \mathbf{x} (Drignei, 2010). Furthermore, the output position t is an intrinsic variable and is of no interest from a sensitivity analysis perspective. With carefully designed kernels in Sec. 3.2, the effects $\{f_{\mathbf{u}|t}(\mathbf{x}_{\mathbf{u}}, t)\}$ are conditionally orthogonal in L_2 at any output position t , which ensures model identifiability. Because of these properties above, the proposed model $f(\mathbf{x}, t)$ in Eq. (10) is called the FOAGP model.

3.2 Functional-Output Orthogonal Additive Kernel

To achieve the orthogonality between effects $\{f_{\mathbf{u}|t}(\mathbf{x}_{\mathbf{u}}, t)\}$, specific constraints must be imposed. First, we propose a separable prior process for the effect $f_{\mathbf{u}|t}(\mathbf{x}_{\mathbf{u}}, t)$, which is determined by the following kernel

$$k_{\mathbf{u}|t}((\mathbf{x}, t), (\mathbf{x}', t')) = k_t(t, t') \prod_{i \in \mathbf{u}} k_i(x_i, x'_i), \quad (11)$$

where $k_i(\cdot)$ is the radial kernel of the i th input x_i with an unknown parameter θ_i , $k_t(\cdot)$ is the radial kernel of output position t with an unknown parameter θ_t . The vector of these parameters are denoted by $\boldsymbol{\theta} = [\theta_1, \dots, \theta_d, \theta_t]^T$. In this study, $k_i(\cdot)$ and $k_t(\cdot)$ are called the input and output kernels, respectively. The kernel structure of the separable prior process in Eq. (11) assumes that there is no input-output interaction because the input and output kernels share no common variables, which is reasonable in many applications (Todescato et al., 2020; Hamelijncx et al., 2021; Lambardi di San Miniato et al., 2022; Zhang et al., 2023).

As the output position t is not involved into the effect decomposition, the orthogonality constraints as provided in Eq. (2) cannot be directly applied to the functional-output

effects $\{f_{\mathbf{u}|t}(\mathbf{x}_{\mathbf{u}}, t)\}$. Instead, consider the conditional orthogonality constraint

$$\int f_{\mathbf{u}|t}(\mathbf{x}_{\mathbf{u}}, t) dF_i(x_i) = 0 \quad (12)$$

for any $i \in \mathbf{u}$ and output position t . We first determine the conditional process $f_{i|t} \mid \{\int f_{i|t}(x_i, t) dF_i(x_i) = 0\}$ of the main effect $f_{i|t}(x_i, t)$, followed by the conditional process $f_{\mathbf{u}|t} \mid \{\int f_{\mathbf{u}|t}(\mathbf{x}_{\mathbf{u}}, t) dF_i(x_i) = 0\}$ of the interaction effect $f_{\mathbf{u}|t}(\mathbf{x}_{\mathbf{u}}, t)$. To determine the first-order conditional process

$$f_{i|t} \mid \left\{ \int f_{i|t}(x_i, t) dF_i(x_i) = 0 \right\}, \quad (13)$$

the following theorem is proposed.

Theorem 1. *Suppose the separable prior process $f_{i|t}$ is a GP determined by the kernel $k_i(\cdot)k_t(\cdot)$. Under the assumption that x_i and t are independent, the conditional process $f_{i|t} \mid \{\int f_{i|t}(x_i, t) dF_i(x_i) = 0\}$ is also a GP determined by a re-constructed kernel $\tilde{k}_i(\cdot)k_t(\cdot)$, where*

$$\tilde{k}_i(x_i, x'_i) = k_i(x_i, x'_i) - \frac{\mathbb{E}_x[k_i(x, x_i)] \mathbb{E}_x[k_i(x, x'_i)]}{\mathbb{E}_{x, x'}[k_i(x, x')]}. \quad (14)$$

Theorem 1 not only establishes that the conditional process follows a GP, but also provides the analytical formula of the re-constructed kernel. The re-constructed kernels $\{\tilde{k}_i(\cdot)\}$ are called orthogonal kernels. These orthogonal kernels $\{\tilde{k}_i(\cdot)\}$ are identical to those obtained by Durrande et al. (2013); Plumlee and Joseph (2018) due to the assumption of no input-output interactions. Moreover, previous proofs for computer experiments with scalar outputs often rely on reproducing kernel Hilbert spaces or stochastic processes, which can be less intuitive and may not be directly extended to functional-output cases. In contrast, this study provides a proof for functional-output computer experiments based on the posterior distribution of the GP, offering a more accessible and practical approach. In practice, the expectations $\mathbb{E}_x[k_i(x, x_i)]$ and $\mathbb{E}_{x, x'}[k_i(x, x')]$ can be estimated using the

training data as an empirical distribution (Lu et al., 2022).

It can be shown that the orthogonal kernels $\{\tilde{k}_i(\cdot)\}$ are positive semi-definite (Plumlee and Joseph, 2018). Moreover, these orthogonal kernels $\{\tilde{k}_i(\cdot)\}$ are data-driven and nonlinear, allowing them to capture the underlying data distribution and enable accurate regression. Furthermore, these orthogonal kernels $\{\tilde{k}_i(\cdot)\}$ are generally non-isotropic, non-stationary and can take both positive and negative values, enhancing their flexibility in modeling intricate relationships (Lu et al., 2022).

Theorem 1 can be extended to the high-order conditional process $f_{\mathbf{u}|t} \mid \left\{ \int f_{\mathbf{u}|t}(\mathbf{x}_{\mathbf{u}}, t) dF_i(x_i) = 0, \forall i \in \mathbf{u} \right\}$ of the interaction effect $f_{\mathbf{u}|t}$ with minor modifications. This extension leverages the proposed separable prior process, which simplifies the enforcement of the conditional orthogonality constraint. As a result, the conditional process $f_{\mathbf{u}|t} \mid \left\{ \int f_{\mathbf{u}|t}(\mathbf{x}_{\mathbf{u}}, t) dF_i(x_i) = 0, \forall i \in \mathbf{u} \right\}$ of the interaction effect $f_{\mathbf{u}|t}$ also follows a GP determined by a re-constructed kernel $\tilde{k}_{\mathbf{u}|t}(\cdot)$, where

$$\tilde{k}_{\mathbf{u}|t}((\mathbf{x}_{\mathbf{u}}, t), (\mathbf{x}'_{\mathbf{u}}, t')) = k_t(t, t') \prod_{i \in \mathbf{u}} \tilde{k}_i(x_i, x'_i). \quad (15)$$

It is worth noting that the re-constructed kernel $\tilde{k}_{i|t}(\cdot) = \tilde{k}_i(\cdot) k_t(\cdot)$ in Theorem 1 also follows the structure in Eq. (15). The proposed kernels $\{\tilde{k}_{\mathbf{u}|t}(\cdot)\}$ are called functional-output orthogonal additive kernels. For the remainder of this study, the notation $f_{\mathbf{u}|t}(\mathbf{x}_{\mathbf{u}}, t)$ is used to denote the conditional process $f_{\mathbf{u}|t} \mid \left\{ \int f_{\mathbf{u}|t}(\mathbf{x}_{\mathbf{u}}, t) dF_i(x_i) = 0 \right\}$ for simplicity. It can be shown that the proposed kernels enable all the effects $\{f_{\mathbf{u}|t}\}$ to satisfy the conditional orthogonality constraints in Eq. (12). Since each pair of the effects contains at least one non-common variable, it can be shown that the conditional GPs are conditionally orthogonal in L_2 space, which guarantees the identifiability of the proposed FOAGP model.

3.3 Parameter Estimation

Consider a dataset $\{\mathbf{X}, \mathbf{T}, \mathbf{y}\}$ consisting of N samples in a d -dimensional space, where $\mathbf{X} = [\mathbf{x}_1, \dots, \mathbf{x}_N]^\top = (x_{uv})_{N \times d}$ is the input point, $\mathbf{T} = [t_1, \dots, t_N]^\top$ is the measured output position, and $\mathbf{y} = [y_1, \dots, y_N]^\top$ is the corresponding output. Let $\mathbf{X}_i = [x_{1i}, \dots, x_{Ni}]^\top$ denote the i th column of \mathbf{X} . The input kernel matrix of \mathbf{X}_i and output kernel matrix are denoted by $\mathbf{K}_i = \tilde{k}_i(\mathbf{X}_i, \mathbf{X}_i) = [\tilde{k}_i(x_{ui}, x_{vi})]_{u,v \in \{1, \dots, N\}}$ and $\mathbf{K}_t = k_t(\mathbf{T}, \mathbf{T}) = [k_t(t_u, t_v)]_{u,v \in \{1, \dots, N\}}$, respectively. The covariance matrix of FOAGP can be rewritten into the Hadamard product of $d + 1$ matrices as

$$\sigma^2 \mathbf{K} = \sigma^2 \left(\delta_0^2 \mathbf{I}_N + \delta_t^2 \mathbf{K}_t \odot \left(\bigodot_{i=1}^d (\mathbf{1}_N \mathbf{1}_N^\top + \delta_i^2 \mathbf{K}_i) \right) \right), \quad (16)$$

where \odot denotes the Hadamard product, \mathbf{I}_N is the $N \times N$ identity matrix, $\mathbf{1}_N$ is an $N \times 1$ vector consisting of N ones, and $\boldsymbol{\delta} = [\delta_0, \delta_1, \dots, \delta_d, \delta_t]^\top$ are parameters to adjust the relative variance across dimensions. The time complexity of computing \mathbf{K} in Eq. (16) is $O(N^2 d)$, making the FOAGP modeling comparable to the standard GP modeling.

Denote the parameters of the kernels by $\boldsymbol{\theta}$ and let $\boldsymbol{\phi} = \{\boldsymbol{\delta}, \boldsymbol{\theta}\}$. Parameter estimation is achieved by maximizing the log marginal likelihood (up to a constant):

$$\ell(\sigma^2, \boldsymbol{\phi}) = -\frac{1}{2} \left(\log |\sigma^2 \mathbf{K}| + \frac{\mathbf{y}^\top \mathbf{K}^{-1} \mathbf{y}}{\sigma^2} \right). \quad (17)$$

Given $\boldsymbol{\phi}$, maximizing the log-likelihood is equivalent to solving the equation that the derivative of the log-likelihood with respect to σ^2 equals to zero. Thus, the parameter estimator of σ^2 is

$$\hat{\sigma}^2 = \frac{1}{N} \mathbf{y}^\top \mathbf{K}^{-1} \mathbf{y}. \quad (18)$$

Finally, the parameter $\boldsymbol{\phi}$ can be numerically optimized by minimizing

$$\hat{\boldsymbol{\phi}} = \underset{\boldsymbol{\phi}}{\operatorname{argmin}} \{ N \log \hat{\sigma}^2 + \log |\mathbf{K}| \}, \quad (19)$$

which can be solved with the gradient descent algorithms (Lophaven et al., 2002).

When the functional outputs are collected at grid output position $\{\tau_v\}_{v=1}^n$ for each input $\chi_u \in \mathbb{R}^d$, where $u = 1, \dots, m$ and $N = mn$, the Hadamard product in Eq. (16) can be replaced by the Kronecker product. Specifically, the covariance matrix can be rewritten as

$$\sigma^2 \mathbf{K} = \sigma^2 \left(\delta_0^2 \mathbf{I}_N + \delta_t^2 \mathbf{R}_t \otimes \left(\bigodot_{i=1}^d (\mathbf{1}_m \mathbf{1}_m^\top + \delta_i^2 \mathbf{R}_i) \right) \right) = \sigma^2 (\delta_0^2 \mathbf{I}_N + \mathbf{C}_t \otimes \mathbf{C}_x), \quad (20)$$

where \otimes denotes the Kronecker product, $\mathbf{R}_t = [k_t(\tau_u, \tau_v)]_{u,v \in \{1, \dots, n\}}$, $\mathbf{R}_i = [\tilde{k}_i(\chi_{ui}, \chi_{vi})]_{u,v \in \{1, \dots, m\}}$, $\mathbf{C}_t = \delta_t^2 \mathbf{R}_t$, and $\mathbf{C}_x = \bigodot_{i=1}^d (\mathbf{1}_m \mathbf{1}_m^\top + \delta_i^2 \mathbf{R}_i)$. Applying Eigen decomposition to \mathbf{C}_t and \mathbf{C}_x gives $\mathbf{C}_t = \mathbf{U} \mathbf{D} \mathbf{U}^\top$ and $\mathbf{C}_x = \mathbf{V} \mathbf{A} \mathbf{V}^\top$, where \mathbf{U} and \mathbf{V} are orthogonal matrices, and \mathbf{D} and \mathbf{A} are diagonal matrices containing the eigenvalues of \mathbf{C}_t and \mathbf{C}_x , respectively. By applying the Eigen decomposition, the correlation matrix \mathbf{K} can be rewritten as

$$\mathbf{K} = (\mathbf{U} \otimes \mathbf{V}) (\delta_0^2 \mathbf{I} + \mathbf{D} \otimes \mathbf{A}) (\mathbf{U} \otimes \mathbf{V})^\top,$$

which implies

$$\begin{cases} |\mathbf{K}| &= |\delta_0^2 \mathbf{I} + \mathbf{D} \otimes \mathbf{A}| = |\mathbf{S}| \\ \mathbf{K}^{-1} &= (\mathbf{U} \otimes \mathbf{V}) \mathbf{S}^{-1} (\mathbf{U} \otimes \mathbf{V})^\top \end{cases}, \quad (21)$$

where $\mathbf{S} = \delta_0^2 \mathbf{I} + \mathbf{D} \otimes \mathbf{A}$ is also a diagonal matrix. These results in Eq. (21) significantly accelerate the computation of $|\mathbf{K}|$ and \mathbf{K}^{-1} from $O(N^3)$ to $O(m^3 + n^3)$. By plugging Eq. (21) into Eq. (18), the parameter estimator of σ^2 becomes

$$\hat{\sigma}^2 = \frac{1}{N} (\text{Vec}(\mathbf{V}^\top \mathbf{Y} \mathbf{U}))^\top \mathbf{S}^{-1} \text{Vec}(\mathbf{V}^\top \mathbf{Y} \mathbf{U}). \quad (22)$$

In the above equation, \mathbf{Y} is the matricization (Zhang, 2017) of \mathbf{y} , i.e.,

$$\mathbf{Y} = \begin{bmatrix} y_{11} & \cdots & y_{1n} \\ \vdots & \ddots & \vdots \\ y_{m1} & \cdots & y_{mn} \end{bmatrix},$$

where y_{uv} is the measurement of $f(\mathbf{x}, t)$ of the input \mathbf{x}_u at output position τ_v . Vec denotes the vectorization that converts a matrix into a vector by sequentially arranging its columns one after the other into a single vector (Zhang, 2017). Given the inverse correlation matrix \mathbf{K}^{-1} , Eq. (22) reduces the time complexity of estimating σ^2 from $O(N^2)$ of Eq. (18) to $O(N(m+n))$. Finally, by plugging Eq. (21) into Eq. (19), the parameter ϕ can be numerically optimized by minimizing

$$\hat{\phi} = \underset{\phi}{\operatorname{argmin}} \{N \log \hat{\sigma}^2 + \log |\mathbf{S}|\}. \quad (23)$$

The use of the Kronecker product (Stegle et al., 2011) significantly reduces the computational complexity of matrix inversion and determinant computations, which is demonstrated on a dataset comprising millions of outputs in the real case study discussed in Sec. 5.

3.4 Functional-Output Effect Decomposition

FOED provides theoretical support for variance decomposition in FOFANOVA and reveals how input variables influence functional outputs, facilitating the understanding of input-output relationships. Moreover, its additive orthogonal structure improves both model interpretability and predictive performance (Duvenaud et al., 2011; Durrande et al., 2012; Sung et al., 2020), providing a comprehensive understanding of complex black-box computer experiments.

Given a new input point \mathbf{x} at output position t , the model prediction $f(\mathbf{x}, t)$ is given by

$$\hat{f}(\mathbf{x}, t) = \left(\delta_t^2 \mathbf{k}_t \odot \left(\bigodot_{i=1}^d (\delta_i^2 \mathbf{k}_i + \mathbf{1}_N) \right) \right)^\top \boldsymbol{\gamma},$$

where $\mathbf{k}_i = \tilde{k}_i(x_i, \mathbf{X}_i) = [\tilde{k}_i(x_i, x_{ui})]_{u \in \{1, \dots, N\}}$, $\mathbf{k}_t = k_t(t, \mathbf{T}) = [k_t(t, t_v)]_{v \in \{1, \dots, N\}}$, and $\boldsymbol{\gamma} = \mathbf{K}^{-1} \mathbf{y}$. The model prediction utilizes the same Hadamard product structure of the covariance matrix \mathbf{K} in Eq. (16), and the time complexity of the model prediction is $O(Nd)$, making the FOAGP prediction also comparable to the standard GP prediction. The prediction $\hat{f}(\mathbf{x}, t)$ can be easily decomposed into 2^d effect predictions $\{\hat{f}_{\mathbf{u}|t}(\mathbf{x}_{\mathbf{u}}, t)\}$, which is given by

$$\hat{f}_{\mathbf{u}|t}(\mathbf{x}_{\mathbf{u}}, t) = \left(\delta_t^2 \mathbf{k}_t \odot \left(\bigodot_{i \in \mathbf{u}} \delta_i^2 \mathbf{k}_i \right) \right)^\top \boldsymbol{\gamma}. \quad (24)$$

The time complexity of computing $\hat{f}_{\mathbf{u}|t}(\mathbf{x}_{\mathbf{u}}, t)$ remains $O(Nd)$, which is identical to the time complexity of model prediction.

When the functional-output outputs are collected at grid output position, the prediction of $f(\mathbf{x}, t)$ and $f_{\mathbf{u}|t}(\mathbf{x}_{\mathbf{u}}, t)$ can be rewritten as

$$\begin{cases} \hat{f}(\mathbf{x}, t) &= \left(\delta_t^2 \mathbf{r}_t \otimes \left(\bigodot_{i=1}^d (\delta_i^2 \mathbf{r}_i + \mathbf{1}_m) \right) \right)^\top \boldsymbol{\gamma} \\ \hat{f}_{\mathbf{u}|t}(\mathbf{x}_{\mathbf{u}}, t) &= \left(\delta_t^2 \mathbf{r}_t \otimes \left(\bigodot_{i \in \mathbf{u}} \delta_i^2 \mathbf{r}_i \right) \right)^\top \boldsymbol{\gamma} \end{cases}, \quad (25)$$

where $\mathbf{r}_t = [k_t(t, \tau_v)]_{v \in \{1, \dots, n\}}$ and $\mathbf{r}_i = [\tilde{k}_i(x_i, \chi_{ui})]_{u \in \{1, \dots, m\}}$. The time complexity of the computing $\hat{f}_{\mathbf{u}|t}(\mathbf{x}_{\mathbf{u}}, t)$ is further reduced to $O(m(n+d))$.

Due to the absence of input-output interactions, the effect predictions $\{\hat{f}_{\mathbf{u}|t}(\mathbf{x}_{\mathbf{u}}, t)\}$ exactly result in orthogonal FOED, which is summarized in the following Theorem 2.

Theorem 2. *The following properties of FOAGP hold under the assumption that the elements in the vector $[\mathbf{x}^\top, t]^\top$ are mutually independent:*

- (a) *Conditional zero mean:* $\int \hat{f}_{\mathbf{u}|t}(\mathbf{x}_{\mathbf{u}}, t) dF(\mathbf{x}) = 0, \forall \mathbf{u} \neq \emptyset, \forall t.$
- (b) *Conditional orthogonality:* $\int \hat{f}_{\mathbf{u}|t}(\mathbf{x}_{\mathbf{u}}, t) \hat{f}_{\mathbf{v}|t}(\mathbf{x}_{\mathbf{v}}, t) dF(\mathbf{x}) = 0, \forall \mathbf{u} \neq \mathbf{v}, \forall t,$ where

$F(\mathbf{x})$ is the distribution function of \mathbf{x} .

The conditional zero mean of Theorem 2(a), derived from the conditional orthogonal constraints in Eq. (12), ensures that the estimated effects $\left\{ \hat{f}_{\mathbf{u}|t}(\mathbf{x}_{\mathbf{u}}, t) \mid \mathbf{u} \neq \emptyset \right\}$ have zero mean at any output position t , further enabling the estimated mean effect $\hat{f}_0(t)$ accurately represents the mean of the functional output $y(\mathbf{x}, t)$. Additionally, the conditional orthogonality of Theorem 2(b), which directly follows from the conditional zero mean of Theorem 2(a) and the independence assumption, ensures the identifiability of the proposed FOAGP model, improves model interpretability, and facilitates the following variance decomposition in Sec. 3.5. Furthermore, theorem 2 demonstrates that by embedding orthogonal FOED directly into the model structure, FOAGP simultaneously performs FOED during modeling, thereby reducing the time cost associated with the separate decomposition step.

3.5 Global Local Variance Decomposition

Variance decomposition lies at the core of FOFANOVA, quantifying the contribution of each input variable to the overall variability of functional outputs. Local variance decomposition assesses input importance at individual output positions, while global variance decomposition evaluates contributions across the entire output domain. Leveraging the full potential of orthogonal FOED in Theorem 2, the local variance decomposition and global variance decomposition of FOAGP are established in the following Theorem 3, offering both local and global insights within a unified sensitivity analysis framework.

Theorem 3. *The following properties of FOAGP hold under the assumption that the elements in the vector $[\mathbf{x}^\top, t]^\top$ are mutually independent:*

- (a) *Local variance decomposition:* $\mathbb{V}_{\mathbf{x}} \left(\hat{f}(\mathbf{x}, t) \right) = \sum_{\mathbf{u} \subseteq \mathcal{D}} \mathbb{V}_{\mathbf{x}_{\mathbf{u}}} \left(\hat{f}_{\mathbf{u}|t}(\mathbf{x}_{\mathbf{u}}, t) \right), \forall t.$
- (b) *Global variance decomposition:* $\mathbb{E}_t \left[\mathbb{V}_{\mathbf{x}} \left(\hat{f}(\mathbf{x}, t) \right) \right] = \sum_{\mathbf{u} \subseteq \mathcal{D}} \mathbb{E}_t \left[\mathbb{V}_{\mathbf{x}_{\mathbf{u}}} \left(\hat{f}_{\mathbf{u}|t}(\mathbf{x}_{\mathbf{u}}, t) \right) \right].$

The local variance decomposition is validated through the conditional mean and the conditional orthogonality in Theorem 2. The global variance decomposition is then ob-

tained by taking the expectation with respect to output position t of the local variance decomposition. While the global variance decomposition provides an overall measure of effect significance, the local variance decomposition provides a finer-grained perspective. Consider the following example: Suppose we have two local variance $\sin t + 1$ and $\sin(10t) + 1$ of two different effects over the interval $[0, 2\pi]$, as illustrated in Fig. 1. The global variance of both yields 1, offering no distinction information between the two different effects. This highlights that effects with different local variances can share the same global variance. Integrating 3(a) and Theorem 3(b) introduces a novel, comprehensive approach to the variance decomposition of functional outputs, which we refer to as global local variance decomposition. Building on the global local variance decomposition, we then develop the global local sensitivity analysis and deduce the analytical formulas of the global local sensitivity indices along with their corresponding estimators for practice.

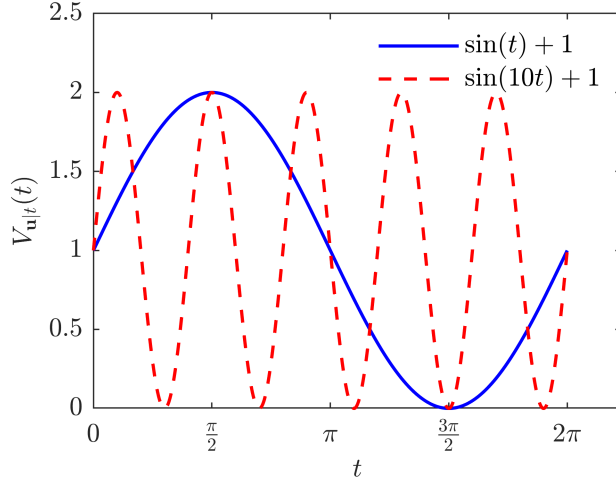


Figure 1: Two different local variance with the same global variance.

The local variances of $\hat{f}_{u|t}(\mathbf{x}_u, t)$ and $\hat{f}(\mathbf{x}, t)$ at output position t are denoted by $V_{u|t}(t) = \mathbb{V}_{\mathbf{x}_u}(\hat{f}_{u|t}(\mathbf{x}_u, t))$ and $V_t(t) = \mathbb{V}_{\mathbf{x}}(\hat{f}(\mathbf{x}, t))$, respectively. The local Sobol' indices of \mathbf{x}_u at output position t are defined as

$$\mathcal{S}_{u|t}(t) = \frac{V_{u|t}(t)}{V_t(t)}, \quad (26)$$

which are also called the local sensitivity indices. Due to the local variance decomposition in Theorem 3(a), we can express the denominator $V_t(t)$ in Eq. (26) as $\sum_{\mathbf{u} \subseteq \mathcal{D}} V_{\mathbf{u}|t}(t)$. Thus, the local Sobol' indices $\mathcal{S}_{\mathbf{u}|t}(t)$ falls within the range $[0, 1]$. Additionally, to obtain the local Sobol' indices $\mathcal{S}_{\mathbf{u}|t}(t)$, we only need to compute $V_{\mathbf{u}|t}(t)$ and normalize them so that their sum equals 1.

The ECV of $\hat{f}_{\mathbf{u}|t}(\mathbf{x}_{\mathbf{u}}, t)$ and $\hat{f}(\mathbf{x}, t)$ are defined as $V_{\mathbf{u}} = \mathbb{E}_t[V_{\mathbf{u}|t}(t)]$ and $V = \mathbb{E}_t[V_t(t)]$, respectively. The ECV averages the local variance over the whole output domain, so we also call it the global variance. The ECV sensitivity indices (Drignei, 2010) of $\mathbf{x}_{\mathbf{u}}$ are defined as

$$\mathcal{S}_{\mathbf{u}} = \frac{V_{\mathbf{u}}}{V}, \quad (27)$$

which we also refer to as the global sensitivity indices in this study. Similar to the local sensitivity analysis, by leveraging the global variance decomposition in Theorem 3(b), we can express the denominator V in Eq. (27) as $\sum_{\mathbf{u} \subseteq \mathcal{D}} V_{\mathbf{u}}$. Again, we only need to compute the ECV $V_{\mathbf{u}}$ of each estimated effect $\hat{f}_{\mathbf{u}|t}(\mathbf{x}_{\mathbf{u}}, t)$, and then normalize them so that their sum equals 1, completing the calculation of the ECV sensitivity indices $\mathcal{S}_{\mathbf{u}}$.

Within the FOAGP framework, the conditional variance $V_{\mathbf{u}|t}(t)$ and the global variance $V_{\mathbf{u}}$ can be derived analytically, which is summarized in the following theorem 4.

Theorem 4. *Under the assumption that the elements in the vector $[\mathbf{x}^\top, t]^\top$ are mutually independent, the local variance $V_{\mathbf{u}|t}(t)$ in Eq. (26) and the global variance $V_{\mathbf{u}}$ in Eq. (27) have analytical formulas within the FOAGP framework, that is,*

$$V_{\mathbf{u}|t}(t) = \gamma^\top \left((\delta_t^4 \mathbf{k}_t \mathbf{k}_t^\top) \odot \left(\bigodot_{i \in \mathbf{u}} \delta_i^4 \mathbb{E}_{x_i} [\mathbf{k}_i \mathbf{k}_i^\top] \right) \right) \gamma, \quad (28)$$

and

$$V_{\mathbf{u}} = \gamma^\top \left(\delta_t^4 \mathbb{E}_t [\mathbf{k}_t \mathbf{k}_t^\top] \odot \left(\bigodot_{i \in \mathbf{u}} \delta_i^4 \mathbb{E}_{x_i} [\mathbf{k}_i \mathbf{k}_i^\top] \right) \right) \gamma, \quad (29)$$

where $\mathbb{E}_t [\mathbf{k}_t \mathbf{k}_t^\top] = \int \mathbf{k}_t \mathbf{k}_t^\top dF_t(t)$ and $F_t(t)$ is the CDF of t .

Noting that $\mathbb{E}_{x_i} [\mathbf{k}_i \mathbf{k}_i^\top]$ and $\mathbb{E}_t [\mathbf{k}_t \mathbf{k}_t^\top]$ may not have closed forms due to the unknown distribution of the input \mathbf{x} and output position t , the conditional variance $V_{\mathbf{u}|t}(t)$ and the global variance $V_{\mathbf{u}}$ are difficult to compute directly. In practice we can estimate these variance through the following two estimators

$$\begin{cases} \hat{V}_{\mathbf{u}|t}(t) &= \boldsymbol{\gamma}^\top ((\delta_t^4 \mathbf{k}_t \mathbf{k}_t^\top) \odot (\odot_{i \in \mathbf{u}} (\delta_i^4 \mathbf{K}_i^2 / N))) \boldsymbol{\gamma} \\ \hat{V}_{\mathbf{u}} &= \boldsymbol{\gamma}^\top ((\delta_t^4 \mathbf{K}_t^2 / N) \odot (\odot_{i \in \mathbf{u}} (\delta_i^4 \mathbf{K}_i^2 / N))) \boldsymbol{\gamma} \end{cases}, \quad (30)$$

which uses the training dataset as an empirical distribution. This approach allows for computing sensitivity indices just after model fitting, making FOAGP a consistent and handy sensitivity analysis tool for functional-output computer experiments. Additionally, all estimators for sensitivity analysis rely solely on the training dataset. These estimators utilize the training dataset to compute local sensitivity indices and global sensitivity indices, enabling global local sensitivity analysis without the prior knowledge about the underlying data distribution.

When the functional outputs are collected at grid output position, the corresponding analytical formulas and estimators can be also derived as follows:

$$\begin{cases} V_{\mathbf{u}|t}(t) &= \text{tr} (\boldsymbol{\Gamma}^\top (\delta_t^4 \mathbf{r}_t \mathbf{r}_t^\top) \boldsymbol{\Gamma} (\odot_{i \in \mathbf{u}} \delta_i^4 \mathbb{E}_{x_i} [\mathbf{r}_i \mathbf{r}_i^\top])) \\ \hat{V}_{\mathbf{u}|t}(t) &= \text{tr} (\boldsymbol{\Gamma}^\top (\delta_t^4 \mathbf{r}_t \mathbf{r}_t^\top) \boldsymbol{\Gamma} (\odot_{i \in \mathbf{u}} (\delta_i^4 \mathbf{R}_i^2 / m))) \\ V_{\mathbf{u}} &= \text{tr} (\boldsymbol{\Gamma}^\top (\delta_t^4 \mathbb{E}_t [\mathbf{r}_t \mathbf{r}_t^\top]) \boldsymbol{\Gamma} (\odot_{i \in \mathbf{u}} \delta_i^4 \mathbb{E}_{x_i} [\mathbf{r}_i \mathbf{r}_i^\top])) \\ \hat{V}_{\mathbf{u}} &= \text{tr} (\boldsymbol{\Gamma}^\top (\delta_t^4 \mathbf{R}_t^2 / n) \boldsymbol{\Gamma} (\odot_{i \in \mathbf{u}} (\delta_i^4 \mathbf{R}_i^2 / m))) \end{cases}, \quad (31)$$

where $\boldsymbol{\Gamma}$ is the matricization of $\boldsymbol{\gamma}$ (Zhang, 2017). Given that the trace operation depends only on the diagonal elements of a matrix, the full result of the matrix multiplication is not necessary. The computational efficiency can be significantly enhanced by focusing only on the diagonal elements.

Since the local Sobol’ indices in Eq. (26) remain invariant under the bijective transformation (Owen and Priour, 2017), the global sensitivity indices derived based on them also retain this property. Therefore, the numerical stability of the FOAGP framework can be further enhanced by utilizing any bijective transformation of the data before training, such as utilizing the normalizing flow (Papamakarios et al., 2021) or mapping the input spaces to $[0, 1]^{d+1}$ with a uniform distribution. The latter transformation will be applied to the real case study discussed in Sec. 5.

While ECV sensitivity indices derived from global variance decomposition provide an overall measure of effect significance, local Sobol’ indices based on local variance decomposition provide detailed insight into the local effect significance, enabling a more comprehensive sensitivity analysis. By integrating these two types of sensitivity indices, we refer to this approach as global local sensitivity analysis. Combined with the global local sensitivity analysis, FOAGP forms a unified data-driven implementation of FOFANOVA for complex black-box computer experiments.

4 Simulation Study

In this section, we apply FOAGP on two simulations to demonstrate its efficiency in orthogonal FOED and variance decomposition. Specifically, we compare the FOED of FOAGP with HDMR in Eq. (6), where Legendre polynomials—orthogonal polynomials on $[-1, 1]$ —are used as the basis functions. Then, we use FOAGP to perform variance decomposition and compare the results with theoretical variance decomposition. The mean trend is extracted for numerical optimization of FOAGP (Burt et al., 2019; Katzfuss et al., 2020), which is also aligned with the set of HDMR (Cheng and Lu, 2019). For HDMR, the input spaces are mapped to $[-1, 1]^3$ with a uniform distribution before training, using inverse of CDF, scaling, and translation.

Example 1. To understand how FOAGP works, we first consider the toy example

$f(x_1, x_2, t) = 1 + 2t + x_1t + 2x_2t + x_1x_2t$. To facilitate theoretical calculations and enable comparison with the fitted results, the input space is set to be \mathbb{R}^3 with a standard ternary normal distribution. White noise $\epsilon \sim \mathcal{N}(0, 0.1^2)$ is added to the data generation model. Example 1 is linear in each input variable and interaction, the importance of each effect directly proportional to its coefficients. Given the input variables follow the same distribution, the variable x_2 with a larger coefficient should have a higher variance and consequently higher sensitivity indices.

The theoretical FOED is easy to derive because each term involving x 's in Example 1 is an odd function with respect to each input variable x_i : $f_0(t) = 1+2t$, $f_1(x_1, t) = x_1t$, $f_2(x_2, t) = 2x_2t$, $f_{12}(x_1, x_2, t) = x_1x_2t$. In addition, the local variance and ECV sensitivity indices can be easily computed: $V_{1|t}(t) = t^2$, $V_{2|t}(t) = 4t^2$, $V_{12|t}(t) = t^2$, $\mathcal{S}_1 = 0.1667$, $\mathcal{S}_2 = 0.6667$, $\mathcal{S}_{12} = 0.1667$. These results are consistent with the previous analysis.

Example 2. To further validate the capability of FOAGP, we duplicate the example $f(x_1, x_2, t) = (t + 1)e^{-x_1t} \sin(2\pi t/x_2)$ given by Drignei (2010). The input space is $(x_1, x_2, t) \in [1.0, 2.0] \times [0.9, 1.1] \times [0.2, 2.0]$ with a uniform distribution and white noise $\epsilon \sim \mathcal{N}(0, 0.01^2)$ is added to the data generation model. Example 2 exhibits oscillations with decreasing amplitude. The second term is an exponential decay function, where x_1 and t have a multiplicative effect on the amplitude. The third term is a sinusoidal function of t and x_2 , with the frequency determined by x_2 . Since that the function is rapidly decreasing with respect to x_1 and oscillatory with respect to x_2 , we can expect that the ECV sensitivity index of x_2 will be greater than that of x_1 . Since x_1 and x_2 are in separate product terms, their interaction is likely to be minimal, implying that the ECV sensitivity index \mathcal{S}_{12} of the interaction effect should be small.

Due to the complex structure of Example 2 and non-symmetric input distribution, the theoretical FOED is not trivial and indeed very complicated, not to mention the local variance decomposition. They are computed by Wolfram Mathematica directly and are

not presented here due to space limitations. Based on these results, the theoretical ECV sensitivity indices are obtained: $\mathcal{S}_1 = 0.3251$, $\mathcal{S}_2 = 0.6027$, $\mathcal{S}_{12} = 0.0722$. These results are consistent with the previous analysis. Directly applying the traditional FANOVA, Drignei (2010) obtained $\hat{\phi}_1 = 0.0003$, $\hat{\phi}_2 = 0.0003$, $\hat{\phi}_t = 0.8749$, $\hat{\phi}_{12} = 0.00004$, $\hat{\phi}_{1t} = 0.0389$, $\hat{\phi}_{2t} = 0.0750$, $\hat{\phi}_{12t} = 0.0105$. Clearly the output position t dominates the the variance, overshadowing the importance of the true input variables x_1 and x_2 . Through the relationship between Sobol' indices and ECV sensitivity indices in Eq. (5), Drignei (2010) estimated ECV sensitivity indices by $\hat{\mathcal{S}}_1 = 0.31$, $\hat{\mathcal{S}}_2 = 0.60$, $\hat{\mathcal{S}}_{12} = 0.09$.

4.1 Effect Decomposition

The FOED results using the FOAGP and HDMR are illustrated in the Fig. 2 and Fig. 3. We present the main effects, omitting the interaction effect due to the limitations of the three-dimensional plot. The FOED of FOAGP closely matches the theoretical FOED in both examples, providing a detailed breakdown of functional outputs, while HDMR struggles to fit the theoretical FOED.

The primary reason for the relatively poor performance of HDMR lies in its reliance on predefined basis functions with the truncated order and its parametric structure, which limit its ability to model complex nonlinear relationships. In Example 1, although the function appears simple, the distribution transformation involving the inverse CDF of $\mathcal{N}(0, 1)$ introduces additional complexity to the function, making it difficult for HDMR to accurately capture the intricate relationships. In contrast, the proposed nonparametric FOAGP model, which does not rely on prior knowledge about the underlying data distribution, is more flexible and able to effectively model complex nonlinear relationships.

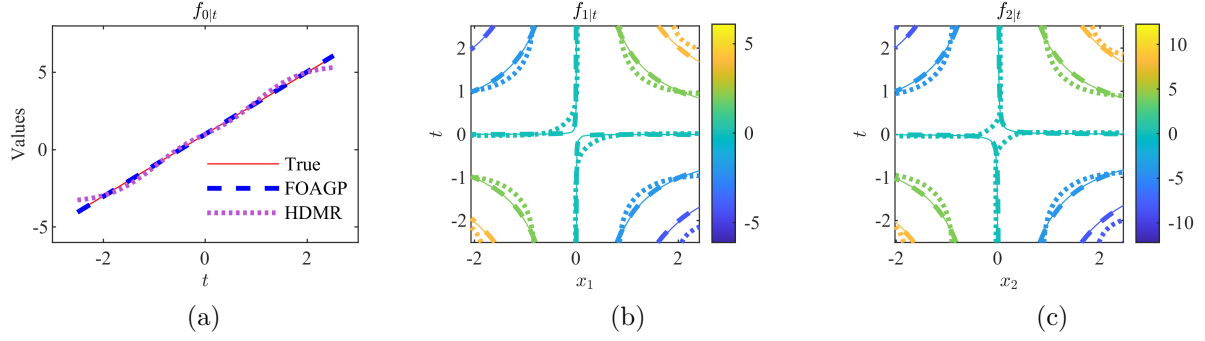


Figure 2: Illustration of FOED of Example 1 using FOAGP and HDMR. The theoretical values are depicted by thin solid lines; the predicted values of FOAGP are depicted by dashed lines; the predicted values of HDMR are depicted by dotted lines.

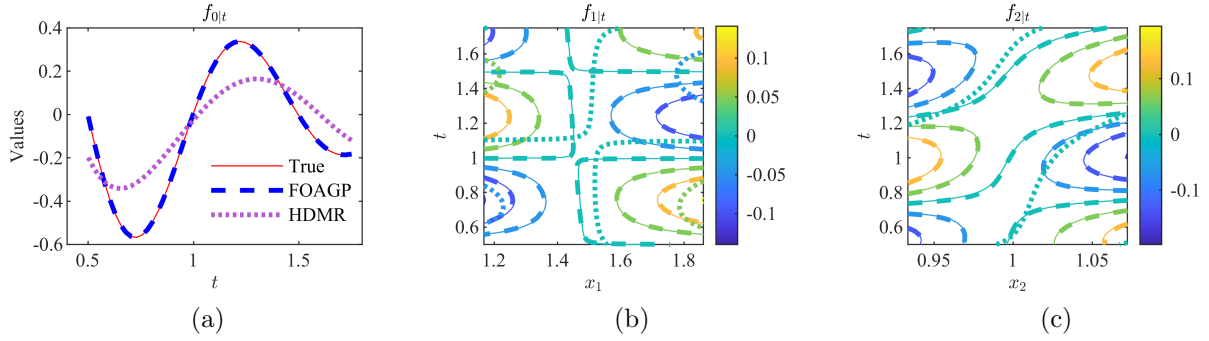


Figure 3: Illustration of FOED of Example 2 using FOAGP and HDMR. The theoretical values are depicted by thin solid lines; the predicted values of FOAGP are depicted by dashed lines; the predicted values of HDMR are depicted by dotted lines.

4.2 Local Variance Decomposition

The local variance decomposition results using FOAGP for both examples are shown in Fig. 4 and Fig. 5. These predicted results using Eq. (30) are very close to the theoretical values, demonstrating the ability of FOAGP to perform local variance decomposition of the functional outputs. By leveraging the entire dataset, the data-driven estimators can accurately estimate the local variance of the functional outputs at any output position. This capacity distinguishes FOAGP from Drignei (2010) method, which applies FANOVA only at fixed output positions to compute the local variance at those fixed output positions.

It is worth noting that in Example 2, while the local variances of the main effects are

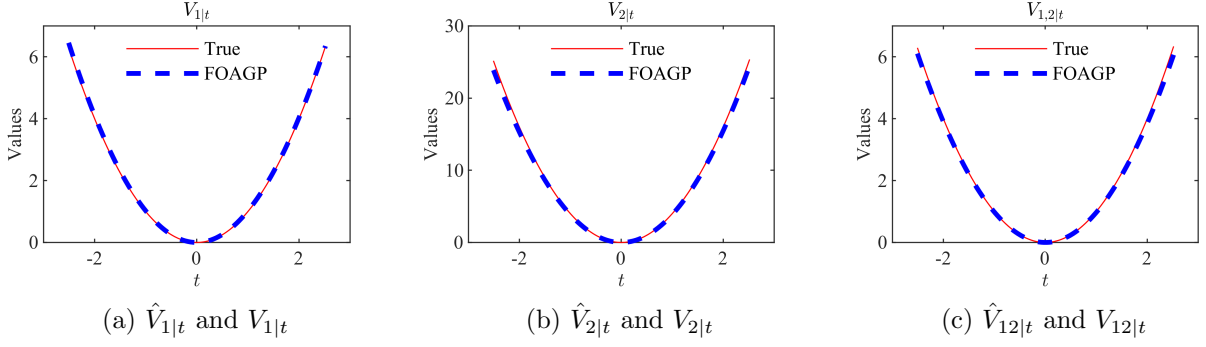


Figure 4: Illustration of the local variance decomposition of Example 1 using FOAGP.

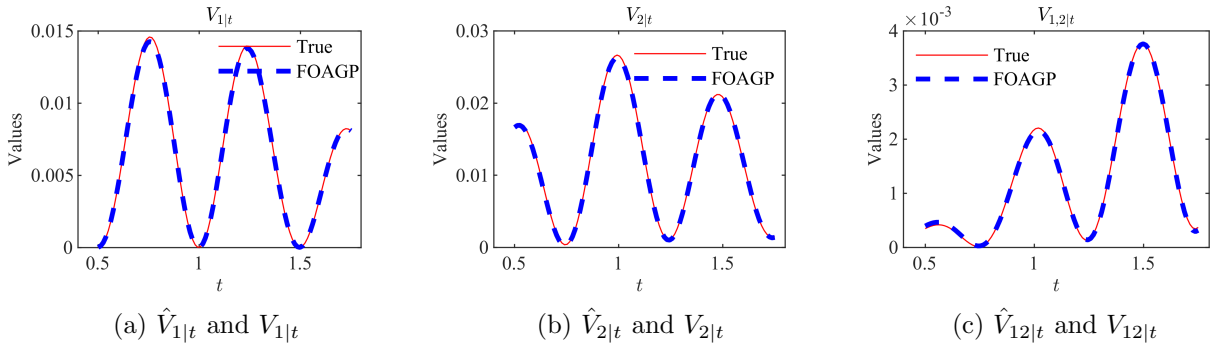


Figure 5: Illustration of the local variance decomposition of the Example 2 using FOAGP.

significantly higher than that of the interaction effect, they almost vanish at some specific points. This highlights the advantage of local variance decomposition in providing a more refined understanding of the underlying variability, whereas relying solely on global variance could obscure the truly important variables at these specific points.

4.3 Global Sensitivity Indices

To demonstrate the effectiveness of FOAGP in estimating global sensitivity indices, we perform simulations on two examples with varying dataset sizes, repeating each simulation 10 times per dataset size. The dataset sizes range from 100 to 5,000, increasing in increments of 100, with a training-to-test ratio of 4:1. The estimated global sensitivity indices are computed using Eq. (27) and Eq. (30). The global sensitivity indices results using FOAGP are shown in Fig. 6, where the thinner dashed horizontal lines represent the theoretical ECV

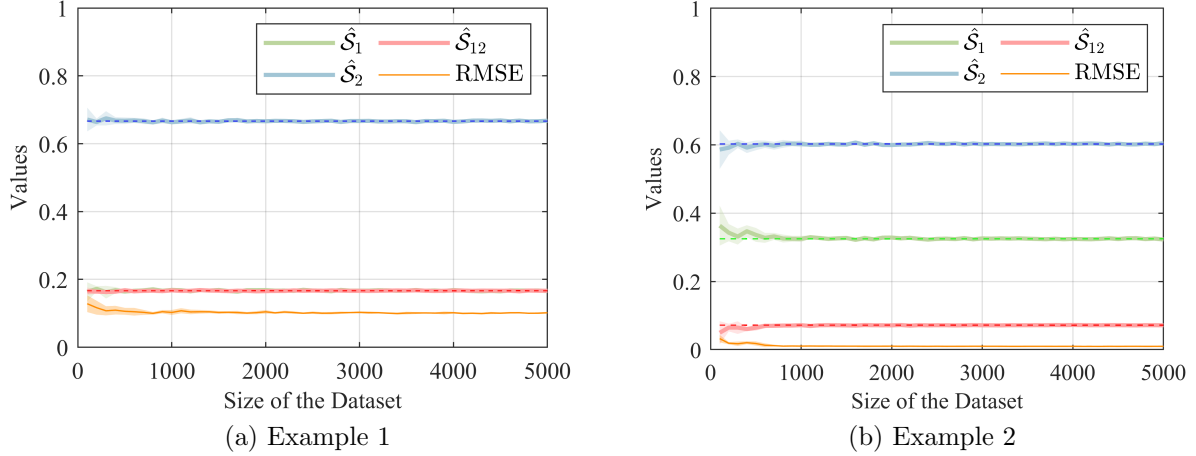


Figure 6: Illustration of the estimated global sensitivity indices and RMSE using FOAGP. Due to the theoretical ECV sensitivity indices $\mathcal{S}_1 = \mathcal{S}_{12}$ in the example 1, the green lines are covered by the red lines in Fig. 6(a).

sensitivity indices, the thicker solid lines represent the estimated global sensitivity indices, the thinner orange line represents the RMSE, and the shaded areas indicate one standard deviation.

In both examples, the estimated global sensitivity indices converge rapidly to the theoretical values, empirically supporting that the data-driven estimators in Eq. (30) are asymptotically unbiased. Similarly, the RMSE also converges quickly in both examples, demonstrating the ability of the nonparametric FOAGP model to accurately capture complicated nonlinear relationships. In example 1, the estimated global sensitivity indices closely match the theoretical values even with very small dataset sizes. This is because the functional output in example 1 shares the same structure as FOAGP in Eq. (10) and is relatively simple.

5 Real Case Study

This section demonstrates the applicability of the proposed FOAGP model with a real case study on fuselage shape control. In order to achieve better dimensional deformation control

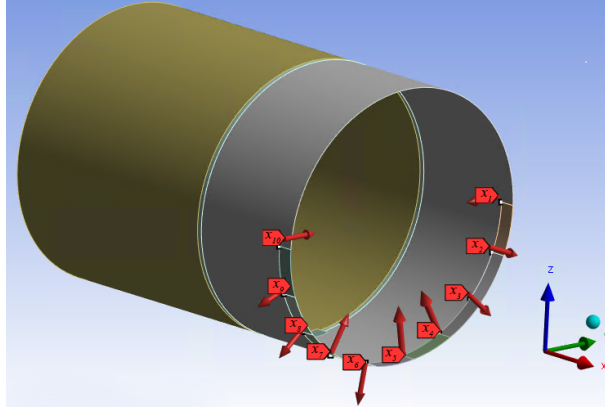


Figure 7: Composite fuselage simulation in Ansys 2024.

around the edge of the fuselage, a shape control system was developed (Wen et al., 2018). As shown in Fig. 7, the system uses 10 actuators uniformly distributed along the lower half of the fuselage in a single plane with the same X-axis, which can push or pull to adjust the in-plane shape of the fuselage. A uniformly sampled dataset for the case study is generated using the finite element model from Wen et al. (2018). The dataset consists of 10,000 instances, each containing 10 forces F_i provided by the actuators, all below 450 pound, where $F_i > 0$ represents a pull and $F_i < 0$ represents a push. Additionally, 100 points are uniformly distributed along the fuselage to measure the deformed radius. The output for each instance represents the deformation at these 100 points, which can be viewed as a functional output of length 100. White noise $\epsilon \sim \mathcal{N}(0, 0.1^2)$ is added to the outputs.

A total of 8,000 instances are randomly selected to train the FOAGP model, with the remaining data forming the test set. The kernel matrix with a Kronecker product structure, as shown in Eq. (20), is utilized to accelerate parameter estimation. Additionally, corresponding predictors and variance estimators in Eq. (25) and Eq. (31) are employed to further improve efficiency. To enhance numerical stability, the forces F_i are scaled from $[-450, 450]$ to $[0, 1]$ by $x_i = (F_i + 450) / 900$ and the angular range is scaled from $[0, 2\pi)$ to $[0, 1)$ by $t = \alpha / (2\pi)$. As discussed in Sec. 3.5, these bijective transformations have no influence on the ECV sensitivity indices. To optimize model performance, a periodic kernel $k_t(t, t') = \exp(-\theta_t^2 \sin^2(\pi(t - t')/T))$ is set for the output position t (MacKay,

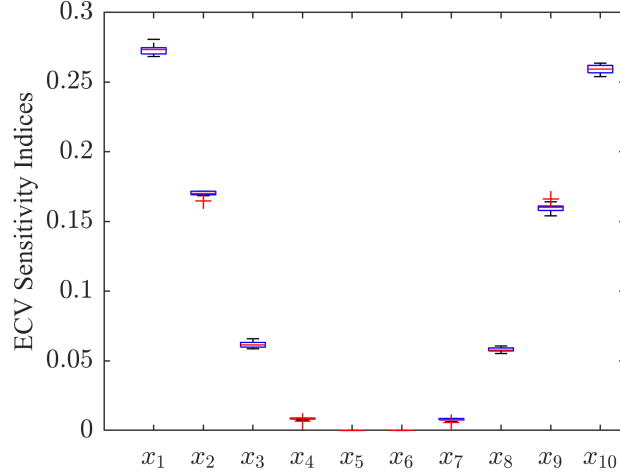


Figure 8: Box plot of the ECV sensitivity indices of the main effects.

1998), with the periodic parameter $T = 1$, while the input kernels remain Gaussian kernels $k_i(x_i, x'_i) = \exp(-(x_i - x'_i)^2 / (2\theta_i^2))$. The experiments are repeated 10 times. Prior to the main experiments, a preliminary test was conducted by incorporating the angle into the traditional FANOVA. The resulting top five Sobol' indices are: $\phi_t = 0.9447, \phi_{1t} = 0.0155, \phi_{10,t} = 0.0142, \phi_{2,t} = 0.0094, \phi_{9,t} = 0.0085$, indicating that the output position t overwhelmingly dominates the variance and overshadows the contributions of the forces.

Fig. 8 shows the box plot of the ECV sensitivity indices for each main effect, with cumulative ECV sensitivity indices of the main effects exceed 0.9977 across all experiments, which indicates that the main effects dominate the variance. This is consistent with the fact that the actuators are positioned within the same plane, where the forces behave as vectors. Consequently, the resulting deformation should approximately follow vector arithmetic rules, with negligible interaction effects. In addition, the actuators located farther from lowest point have a greater influence, while those near the lowest point have minimal influence.

Fig. 9 visualizes the deformation caused by the main effects of the actuators. The edge curves illustrate the main effects of forces on the fuselage shape. Actuators located farther from the lowest point, particularly the 1st and 10th actuators, exert greater and more sym-

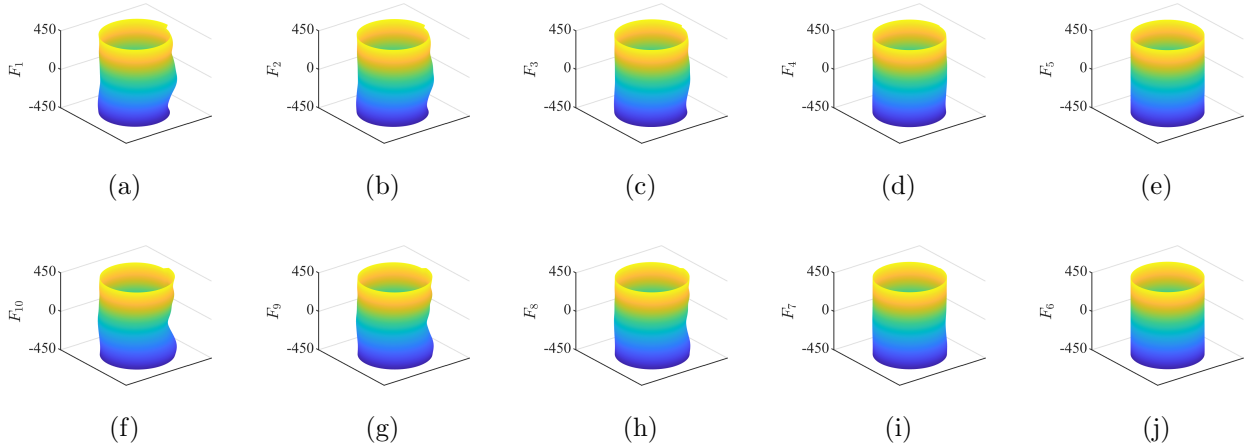


Figure 9: The deformation caused by the main effects of the forces. To illustrate the deformation better, we scale the original radius to 1/10 and the deformation remains unchanged.

metric influences on the fuselage shape due to their mid-height placement. This suggests that focusing on these key actuators can improve control efficiency and system reliability. Conversely, the minimal impact of actuators near the lowest point indicates potential opportunities for system simplification and cost reduction without compromising performance. This understanding enables engineers to prioritize actuator placement strategically, optimizing both the performance and cost-effectiveness in fuselage shape control systems. These results demonstrate the capability of FOAGP to perform orthogonal FOED and sensitivity analysis in real-world scenarios, offering a unified data-driven implementation of FOFANOVA with significant practical value.

6 Conclusions

In this study, we propose the FOAGP model, a novel data-driven, nonlinear, and non-parametric modeling approach for efficient FOED. The FOAGP model fully incorporates high-order effects and embeds FOED directly into model structure, reducing the time cost associated with separate decomposition steps. Utilizing the proposed functional-output

orthogonal additive kernel, FOAGP achieves orthogonal FOED without requiring prior knowledge about the underlying data distribution. Furthermore, a corresponding global local variance decomposition is established within the FOAGP framework, enabling comprehensive global local sensitivity analysis for functional-output computer experiments. The effectiveness of FOAGP is demonstrated through two simulation studies and a real-world case study on fuselage shape control. These experiments validate the model’s capability to perform FOED and accurately quantify variable importance, highlighting FOAGP as a practical and handy tool for FOFANOVA in functional-output computer experiments, and demonstrating its potential values in complex engineering scenarios.

While this study focuses only on one-dimensional functional outputs, the method can be readily extendable to high-dimensional functional output case, which will be explored in the future research. The proposed FOAGP model is under the assumption of no input-output interactions. In scenarios where such interactions exist, the model assumptions may need to be revised. Future work will explore incorporating input-output interactions through frameworks such as generalized FANOVA and Shapley values. Another promising direction involves leveraging functional-output effect decomposition within the context of Bayesian functional optimization, which may open new avenues for efficient optimization in functional spaces.

Acknowledgments

We would like to express our sincere gratitude to Jeff Wu and Jianhua Huang for their fruitful comments for this paper.

References

- Apley, D. W. and Zhu, J. (2020), “Visualizing the Effects of Predictor Variables in Black Box Supervised Learning Models,” *Journal of the Royal Statistical Society: Series B (Statistical Methodology)*, 82, 1059–1086.

- Bolin, D., Verendel, V., Berghauser Pont, M., Stavroulaki, I., Ivarsson, O., and Håkansson, E. (2021), “Functional ANOVA Modelling of Pedestrian Counts on Streets in Three European Cities,” *Journal of the Royal Statistical Society Series A: Statistics in Society*, 184, 1176–1198.
- Burt, D., Rasmussen, C. E., and Wilk, M. V. D. (2019), “Rates of Convergence for Sparse Variational Gaussian Process Regression,” in *Proceedings of the 36th International Conference on Machine Learning*, PMLR, pp. 862–871.
- Centofanti, F., Colosimo, B. M., Grasso, M. L., Menafoglio, A., Palumbo, B., and Vantini, S. (2023), “Robust Functional ANOVA with Application to Additive Manufacturing,” *Journal of the Royal Statistical Society Series C: Applied Statistics*, 72, 1210–1234.
- Chen, H., Covert, I. C., Lundberg, S. M., and Lee, S.-I. (2023), “Algorithms to Estimate Shapley Value Feature Attributions,” *Nature Machine Intelligence*, 5, 590–601.
- Cheng, K. and Lu, Z. (2019), “Time-Variant Reliability Analysis Based on High Dimensional Model Representation,” *Reliability Engineering & System Safety*, 188, 310–319.
- Chiogna, G., Marcolini, G., Engel, M., and Wohlmuth, B. (2024), “Sensitivity Analysis in the Wavelet Domain: A Comparison Study,” *Stochastic Environmental Research and Risk Assessment*, 38, 1669–1684.
- Drignei, D. (2010), “Functional ANOVA in Computer Models With Time Series Output,” *Technometrics*, 52, 430–437.
- Durrande, N., Ginsbourger, D., and Roustant, O. (2012), “Additive Covariance Kernels for High-Dimensional Gaussian Process Modeling,” *Annales de la Faculté des sciences de Toulouse : Mathématiques*, 21, 481–499.
- Durrande, N., Ginsbourger, D., Roustant, O., and Carraro, L. (2013), “ANOVA Kernels and RKHS of Zero Mean Functions for Model-Based Sensitivity Analysis,” *Journal of Multivariate Analysis*, 115, 57–67.
- Duvenaud, D. K., Nickisch, H., and Rasmussen, C. (2011), “Additive Gaussian Processes,” in *Advances in Neural Information Processing Systems*, Curran Associates, Inc., vol. 24.
- Efron, B. and Stein, C. (1981), “The Jackknife Estimate of Variance,” *The Annals of Statistics*, 9, 586–596.
- Fang, K.-T., Li, R., and Sudjianto, A. (2005), *Design and modeling for computer experiments*, Chapman and Hall/CRC.
- Faraway, J. J. (1997), “Regression Analysis for a Functional Response,” *Technometrics*, 39, 254–261.
- Garouani, M. and Bouneffa, M. (2024), “Automated Machine Learning Hyperparameters Tuning through Meta-Guided Bayesian Optimization,” *Progress in Artificial Intelligence*.

- Ginsbourger, D., Roustant, O., Schuhmacher, D., Durrande, N., and Lenz, N. (2016), “On ANOVA Decompositions of Kernels and Gaussian Random Field Paths,” in *Monte Carlo and Quasi-Monte Carlo Methods*, eds. Cools, R. and Nuyens, D., Cham: Springer International Publishing, pp. 315–330.
- Hamelijnck, O., Wilkinson, W., Loppi, N., Solin, A., and Damoulas, T. (2021), “Spatio-Temporal Variational Gaussian Processes,” in *Advances in Neural Information Processing Systems*, Curran Associates, Inc., vol. 34, pp. 23621–23633.
- Hooker, G. (2004), “Discovering Additive Structure in Black Box Functions,” in *Proceedings of the Tenth ACM SIGKDD International Conference on Knowledge Discovery and Data Mining*, Seattle WA USA: ACM, pp. 575–580.
- (2007), “Generalized Functional ANOVA Diagnostics for High-Dimensional Functions of Dependent Variables,” *Journal of Computational and Graphical Statistics*, 16, 709–732.
- Janon, A., Klein, T., Lagnoux, A., Nodet, M., and Prieur, C. (2014), “Asymptotic Normality and Efficiency of Two Sobol Index Estimators,” *ESAIM: Probability and Statistics*, 18, 342–364.
- Jiang, F., Tan, M. H. Y., and Tsui, K.-L. (2021), “Multiple-Target Robust Design with Multiple Functional Outputs,” *IIE Transactions*, 53, 1052–1066.
- Katzfuss, M., Guinness, J., Gong, W., and Zilber, D. (2020), “Vecchia Approximations of Gaussian-Process Predictions,” *Journal of Agricultural, Biological and Environmental Statistics*, 25, 383–414.
- Kimeldorf, G. and Wahba, G. (1971), “Some Results on Tchebycheffian Spline Functions,” *Journal of Mathematical Analysis and Applications*, 33, 82–95.
- Kokoszka, P. and Reimherr, M. (2017), *Introduction to Functional Data Analysis*, Texts in Statistical Science Series, Boca Raton: CRC Press, Taylor & Francis Group.
- Lambardi di San Miniato, M., Bellio, R., Grassetti, L., and Vidoni, P. (2022), “Separable Spatio-Temporal Kriging for Fast Virtual Sensing,” *Applied Stochastic Models in Business and Industry*, 38, 806–829.
- Liu, Q., Tong, N., Wu, X., Han, X., and Chen, C. (2021), “A Generalized Sensitivity Analysis Method Based on Variance and Covariance Decomposition of Summatory Functions for Multi-Input Multi-Output Systems,” *Computer Methods in Applied Mechanics and Engineering*, 385, 114009.
- Liu, Z., Li, Y., Yue, X., and Pan, E. (2024), “Latent Functional Gaussian Process Incorporating Output Spatial Correlations,” *IIE Transactions*, 0, 1–24.
- Lophaven, S. N., Nielsen, H. B., and Søndergaard, J. (2002), *Aspects of the matlab toolbox DACE*, Citeseer.

- Lu, X., Boukouvalas, A., and Hensman, J. (2022), “Additive Gaussian Processes Revisited,” in *Proceedings of the 39th International Conference on Machine Learning*, PMLR, pp. 14358–14383.
- Ma, P., Mondal, A., Konomi, B. A., Hobbs, J., Song, J. J., and Kang, E. L. (2022), “Computer Model Emulation with High-Dimensional Functional Output in Large-Scale Observing System Uncertainty Experiments,” *Technometrics*, 64, 65–79.
- MacKay, D. J. (1998), “Introduction to Gaussian processes,” *NATO ASI Series F Computer and Systems Sciences*, 168, 133–166.
- Marnissi, Y. and Leiber, M. (2024), “A Unified View of FANOVA: A Comprehensive Bayesian Framework for Component Selection and Estimation,” in *Forty-First International Conference on Machine Learning*.
- Muehlenstaedt, T., Roustant, O., Carraro, L., and Kuhnt, S. (2012), “Data-Driven Kriging Models Based on FANOVA-decomposition,” *Statistics and Computing*, 22, 723–738.
- Owen, A. B. (2014), “Sobol’ Indices and Shapley Value,” *SIAM/ASA Journal on Uncertainty Quantification*, 2, 245–251.
- Owen, A. B. and Prieur, C. (2017), “On Shapley Value for Measuring Importance of Dependent Inputs,” *SIAM/ASA Journal on Uncertainty Quantification*, 5, 986–1002.
- Papamakarios, G., Nalisnick, E., Rezende, D. J., Mohamed, S., and Lakshminarayanan, B. (2021), “Normalizing Flows for Probabilistic Modeling and Inference,” *Journal of Machine Learning Research*, 22, 57:2617–57:2680.
- Plumlee, M. and Joseph, V. R. (2018), “Orthogonal Gaussian Process Models,” *Statistica Sinica*, 28, 601–619.
- Rao, A. R. and Reimherr, M. (2023), “Modern Non-Linear Function-on-Function Regression,” *Statistics and Computing*, 33, 130.
- Rougier, J. (2008), “Efficient Emulators for Multivariate Deterministic Functions,” *Journal of Computational and Graphical Statistics*, 17, 827–843.
- Santner, T. J., Williams, B. J., and Notz, W. I. (2018), *The Design and Analysis of Computer Experiments*, Springer Series in Statistics, New York, NY: Springer New York.
- Shi, J. Q., Wang, B., Murray-Smith, R., and Titterton, D. M. (2007), “Gaussian Process Functional Regression Modeling for Batch Data,” *Biometrics*, 63, 714–723.
- Shi, Y., Lu, Z., Li, Z., and Wu, M. (2018), “Cross-Covariance Based Global Dynamic Sensitivity Analysis,” *Mechanical Systems and Signal Processing*, 100, 846–862.
- Sobol’, I. (1993), “Sensitivity estimates for nonlinear mathematical models,” *Math. Model. Comput. Exp.*, 1, 407.

- Sobol', I. M. (1990), "On sensitivity estimation for nonlinear mathematical models," *Matematicheskoe modelirovanie*, 2, 112–118.
- (2001), "Global Sensitivity Indices for Nonlinear Mathematical Models and Their Monte Carlo Estimates," *Mathematics and Computers in Simulation*, 55, 271–280.
- Stegle, O., Lippert, C., Mooij, J. M., Lawrence, N., and Borgwardt, K. (2011), "Efficient Inference in Matrix-Variate Gaussian Models with \backslash textbackslash iid Observation Noise," in *Advances in Neural Information Processing Systems*, Curran Associates, Inc., vol. 24.
- Sung, C.-L., Wang, W., Plumlee, M., and Haaland, B. (2020), "Multiresolution Functional ANOVA for Large-Scale, Many-Input Computer Experiments," *Journal of the American Statistical Association*, 115, 908–919.
- Todescato, M., Carron, A., Carli, R., Pillonetto, G., and Schenato, L. (2020), "Efficient Spatio-Temporal Gaussian Regression via Kalman Filtering," *Automatica*, 118, 109032.
- Wagener, T. and Pianosi, F. (2019), "What Has Global Sensitivity Analysis Ever Done for Us? A Systematic Review to Support Scientific Advancement and to Inform Policy-Making in Earth System Modelling," *Earth-Science Reviews*, 194, 1–18.
- Wang, Z., Xing, W., Kirby, R., and Zhe, S. (2021), "Multi-Fidelity High-Order Gaussian Processes for Physical Simulation," in *Proceedings of The 24th International Conference on Artificial Intelligence and Statistics*, PMLR, pp. 847–855.
- Wen, Y., Yue, X., Hunt, J. H., and Shi, J. (2018), "Feasibility Analysis of Composite Fuselage Shape Control via Finite Element Analysis," *Journal of Manufacturing Systems*, 46, 272–281.
- Xiao, S., Lu, Z., and Wang, P. (2018), "Multivariate Global Sensitivity Analysis for Dynamic Models Based on Wavelet Analysis," *Reliability Engineering & System Safety*, 170, 20–30.
- Yue, Y. R., Bolin, D., Rue, H., and Wang, X.-F. (2019), "Bayesian Generalized Two-way ANOVA Modeling for Functional Data Using INLA," *Statistica Sinica*, 29, 741–767.
- Zhang, J., Crippa, P., Genton, M. G., and Castruccio, S. (2024), "Sensitivity Analysis of Wind Energy Resources with Bayesian Non-Gaussian and Nonstationary Functional ANOVA," *The Annals of Applied Statistics*, 18, 23–41.
- Zhang, J., Ju, Y., Mu, B., Zhong, R., and Chen, T. (2023), "An Efficient Implementation for Spatial–Temporal Gaussian Process Regression and Its Applications," *Automatica*, 147, 110679.
- Zhang, J.-T., Cheng, M.-Y., Wu, H.-T., and Zhou, B. (2019), "A New Test for Functional One-Way ANOVA with Applications to Ischemic Heart Screening," *Computational Statistics & Data Analysis*, 132, 3–17.
- Zhang, X.-D. (2017), *Matrix Analysis and Applications*, Cambridge University Press, 1st ed.

Supplemental Material to “Effect Decomposition of Functional-Output Computer Experiments via Orthogonal Additive Gaussian Processes”

1 Proof

Proof of Theorem 1. Without loss of generality, we assume that the input variable x_i and the time t both lie in the interval $[0, 1]$ with a uniform distribution. If the range of x_i or t is not within $[0, 1]$, a bijective transformation can be applied to map the range to $[0, 1]$. If the distribution of x_i or t are not uniform, the differential dx_i or dt used in the following proof can be replaced by the measure $dF_i(x_i)$ or $dF_t(t)$, respectively.

Given the separable prior process

$$f \sim \mathcal{GP}(\mathbf{0}, k_i k_t),$$

where $f : [0, 1]^2 \rightarrow \mathbb{R}$. Under the grid design on the input space $\left\{ \left(x_{i,u}^{(n)}, t_v^{(n)} \right) \right\}_{u,v=1}^n \subseteq [0, 1]^2$, where $x_{i,u}^{(n)} = u/n$ and $t_v^{(n)} = v/n$, the orthogonality constraint can be approximated by

$$z_v^{(n)} = \int f(x_i, t_v^{(n)}) dx_i \approx \frac{1}{n} \sum_{u=1}^n f(x_{i,u}^{(n)}, t_v^{(n)}) = \mathbf{a}_n^\top \mathbf{f}_v^{(n)},$$

where \mathbf{a}_n is a $n \times 1$ vector comprising all the elements equal to $1/n$, $\mathbf{f}_v^{(n)} =$

$\left[f \left(x_{i,1}^{(n)}, t_v^{(n)} \right), \dots, \left(x_{i,n}^{(n)}, t_v^{(n)} \right) \right]^\top$. Let

$$\mathbf{z}^{(n)} = \begin{bmatrix} z_1^{(n)} \\ \vdots \\ z_n^{(n)} \end{bmatrix} = (\mathbf{I}_n \otimes \mathbf{a}_n)^\top \begin{bmatrix} \mathbf{f}_1^{(n)} \\ \vdots \\ \mathbf{f}_n^{(n)} \end{bmatrix} = (\mathbf{I}_n \otimes \mathbf{a}_n)^\top \mathbf{f}^{(n)},$$

where $\mathbf{f}^{(n)} = \left[\left(\mathbf{f}_1^{(n)} \right)^\top \dots \left(\mathbf{f}_n^{(n)} \right)^\top \right]^\top$. It is easy to show that $\mathbb{V} \left(\mathbf{f}^{(n)} \right) = \mathbf{K}_t^{(n)} \otimes \mathbf{K}_i^{(n)}$, $\mathbb{V} \left(\mathbf{z}^{(n)} \right) = \mathbf{K}_t^{(n)} \otimes \left(\mathbf{a}_n^\top \mathbf{K}_i^{(n)} \mathbf{a}_n \right)$ and $\text{Cov} \left(\mathbf{f}^{(n)}, \mathbf{z}^{(n)} \right) = \mathbf{K}_t^{(n)} \otimes \left(\mathbf{K}_i^{(n)} \mathbf{a}_n \right)$, where $\mathbf{K}_t^{(n)} = \left[k_t \left(t_u^{(n)}, t_v^{(n)} \right) \right]_{u,v=1,\dots,n}$ and $\mathbf{K}_i^{(n)} = \left[k_i \left(x_{i,u}^{(n)}, x_{i,v}^{(n)} \right) \right]_{u,v=1,\dots,n}$. By the definition of Gaussian Process, the joint distribution of $\left(\mathbf{f}^{(n)}, \mathbf{z}^{(n)} \right)$ is Gaussian, and it is easy to show that

$$\begin{bmatrix} \mathbf{f}^{(n)} \\ \mathbf{z}^{(n)} \end{bmatrix} \sim \left(\mathbf{0}, \begin{bmatrix} \mathbf{K}_t^{(n)} \otimes \mathbf{K}_i^{(n)} & \mathbf{K}_t^{(n)} \otimes \left(\mathbf{K}_i^{(n)} \mathbf{a}_n \right) \\ \mathbf{K}_t^{(n)} \otimes \left(\mathbf{a}_n^\top \mathbf{K}_i^{(n)} \right) & \mathbf{K}_t^{(n)} \otimes \left(\mathbf{a}_n^\top \mathbf{K}_i^{(n)} \mathbf{a}_n \right) \end{bmatrix} \right).$$

So the posterior distribution of $\mathbf{f}^{(n)} \mid \{ \mathbf{z}^{(n)} = \mathbf{0} \}$ can be derived

$$\begin{aligned} & \mathbf{f}^{(n)} \mid \{ \mathbf{z}^{(n)} = \mathbf{0} \} \\ & \sim \mathcal{N} \left(\mathbf{0}, \mathbf{K}_t^{(n)} \otimes \mathbf{K}_i^{(n)} - \left(\mathbf{K}_t^{(n)} \otimes \left(\mathbf{K}_i^{(n)} \mathbf{a}_n \right) \right) \left(\mathbf{K}_t^{(n)} \otimes \left(\mathbf{a}_n^\top \mathbf{K}_i^{(n)} \mathbf{a}_n \right) \right)^{-1} \left(\mathbf{K}_t^{(n)} \otimes \left(\mathbf{K}_i^{(n)} \mathbf{a}_n \right)^\top \right) \right) \\ & = \mathcal{N} \left(\mathbf{0}, \mathbf{K}_t^{(n)} \otimes \mathbf{K}_i^{(n)} - \mathbf{K}_t^{(n)} \otimes \frac{\left(\mathbf{K}_i^{(n)} \mathbf{a}_n \right) \left(\mathbf{K}_i^{(n)} \mathbf{a}_n \right)^\top}{\mathbf{a}_n^\top \mathbf{K}_i^{(n)} \mathbf{a}_n} \right) \\ & = \mathcal{N} \left(\mathbf{0}, \mathbf{K}_t^{(n)} \otimes \left(\mathbf{K}_i^{(n)} - \frac{\left(\mathbf{K}_i^{(n)} \mathbf{a}_n \right) \left(\mathbf{K}_i^{(n)} \mathbf{a}_n \right)^\top}{\mathbf{a}_n^\top \mathbf{K}_i^{(n)} \mathbf{a}_n} \right) \right). \end{aligned} \tag{32}$$

For any two points (x_i, t) and (x'_i, t') , there exist two sequences $\left(x_\alpha^{(n)}, t_\xi^{(n)} \right)$ and $\left(x_\beta^{(n)}, t_\eta^{(n)} \right)$

in $[0, 1] \times [0, 1]$ such that when n tends to infinity

$$\left(x_{\alpha}^{(n)}, t_{\xi}^{(n)}\right) \rightarrow \left(x_i, t\right), \text{ and } \left(x_{\beta}^{(n)}, t_{\eta}^{(n)}\right) \rightarrow \left(x'_i, t'\right).$$

It should be noted that here α , β , ξ , and η are dependent on n . The correlation between $\left(x_{\alpha}^{(n)}, t_{\xi}^{(n)}\right)$ and $\left(x_{\beta}^{(n)}, t_{\eta}^{(n)}\right)$ is exactly the $(\xi - 1)n + \alpha$ th row and $(\eta - 1)n + \beta$ th column of the kernel matrix in Eq. (32), i.e.,

$$k_t\left(t_{\xi}^{(n)}, t_{\eta}^{(n)}\right) \left(k\left(x_{\alpha}^{(n)}, x_{\beta}^{(n)}\right) - \frac{\left[\frac{1}{n} \sum_{u=1}^n k\left(x_{i,u}, x_{\alpha}^{(n)}\right)\right] \left[\frac{1}{n} \sum_{v=1}^n k\left(x_{i,v}, x_{\beta}^{(n)}\right)\right]}{\frac{1}{n^2} \sum_{u,v=1}^n k\left(x_{i,u}, x_{i,v}\right)} \right).$$

Taking the limit of $n \rightarrow \infty$ yields

$$\begin{aligned} \tilde{k}_{i|t}\left((x_i, t), (x'_i, t')\right) &= k_t(t, t') \left(k(x_i, x'_i) - \frac{\mathbb{E}_x[k(x, x_i)] \mathbb{E}_{x'}[k(x', x'_i)]}{\mathbb{E}_{x,x'}[k(x, x')]} \right) \\ &= k_t(t, t') \tilde{k}(x_i, x'_i), \end{aligned}$$

where $\tilde{k}(x_i, x'_i)$ is exactly the orthogonal kernel. Taking the limit of $n \rightarrow \infty$ in Eq. (32) gives the conditional GP

$$f_{i|t} \mid \left\{ \int f_{i|t}(x_i, t) dF_i(x_i) = 0 \right\} \sim \mathcal{GP}\left(0, \tilde{k}_i k_t\right),$$

which finishes the proof.

Proof of Theorem 2. The representer theorem (Kimeldorf and Wahba, 1971) shows that the effect prediction $\hat{f}_{u|t}(\mathbf{x}_u, t)$ lies within the span of the corresponding kernel $\tilde{k}_{u|t}(\cdot)$. It suffices to show that the conditional zero mean and conditional orthogonality hold for the proposed kernels $\left\{ \tilde{k}_{u|t}(\cdot) \right\}$. By the construction of the orthogonal kernels $\left\{ \tilde{k}_i(\cdot) \right\}$ in Theorem 1, it is straightforward to verify that $\mathbb{E}_{x_i} \left[\tilde{k}_i(x_i, x'_i) \right] = 0$.

(a) Conditional zero mean: For any fixed point (\mathbf{x}', t') , we have

$$\begin{aligned}
\int k_{\mathbf{u}|t}((\mathbf{x}_{\mathbf{u}}, t), (\mathbf{x}'_{\mathbf{u}}, t')) dF(\mathbf{x}) &= k_t(t, t') \int \prod_{i \in \mathbf{u}} \tilde{k}_i(x_i, x'_i) dF(\mathbf{x}) \\
&= k_t(t, t') \prod_{i \in \mathbf{u}} \int \tilde{k}_i(x_i, x'_i) dF_i(x_i) \\
&= k_t(t, t') \prod_{i \in \mathbf{u}} \mathbb{E}_{x_i} [\tilde{k}_i(x_i, x'_i)] \\
&= 0,
\end{aligned}$$

where the first equality follows from the definition of the proposed kernel $\tilde{k}_{\mathbf{u}|t}(\cdot)$, the second equality leverages the independence of $\{x_i\}$, the third equality uses the definition of expectation, and the last equality is based on the previous result $\mathbb{E}_{x_i} [\tilde{k}_i(x_i, x'_i)] = 0$.

(b) Conditional orthogonality: When either \mathbf{u} or \mathbf{v} is the null set \emptyset , the conditional orthogonality degenerates to the conditional mean. In all other cases, where $\mathbf{u} \neq \mathbf{v}$, there exists $i^* \in \{1, \dots, d\}$ such that $i^* \in \mathbf{u} \Delta \mathbf{v} = (\mathbf{u} \setminus \mathbf{v}) \cup (\mathbf{v} \setminus \mathbf{u})$, where \setminus denotes the set difference and Δ denotes the symmetric difference, meaning $\mathbf{u} \Delta \mathbf{v} \neq \emptyset$. For any fixed point (\mathbf{x}', t') , we have

$$\begin{aligned}
&\int k_{\mathbf{u}|t}((\mathbf{x}_{\mathbf{u}}, t), (\mathbf{x}'_{\mathbf{u}}, t')) k_{\mathbf{v}|t}((\mathbf{x}_{\mathbf{v}}, t), (\mathbf{x}'_{\mathbf{v}}, t')) dF(\mathbf{x}) \\
&= k_t(t, t') \int \left(\prod_{i \in \mathbf{u} \cap \mathbf{v}} [\tilde{k}_i(x_i, x'_i)]^2 \right) \left(\prod_{i \in \mathbf{u} \Delta \mathbf{v}} \tilde{k}_i(x_i, x'_i) \right) \prod_{i \in \mathbf{u} \cup \mathbf{v}} dF_i(x_i) \\
&= k_t(t, t') \left(\prod_{i \in \mathbf{u} \cap \mathbf{v}} \int [\tilde{k}_i(x_i, x'_i)]^2 dF(x_i) \right) \prod_{i \in \mathbf{u} \Delta \mathbf{v}} \int \tilde{k}_i(x_i, x'_i) dF_i(x_i) \\
&= k_t(t, t') \left(\prod_{i \in \mathbf{u} \cap \mathbf{v}} \int [\tilde{k}_i(x_i, x'_i)]^2 dF(x_i) \right) \prod_{i \in \mathbf{u} \Delta \mathbf{v}} \mathbb{E}_{x_i} [\tilde{k}_i(x_i, x'_i)] \\
&= 0.
\end{aligned}$$

The first equality follows from the definition of proposed kernel $\tilde{k}_{\mathbf{u}|t}(\cdot)$, the identity $\mathbf{u} \cup \mathbf{v} = (\mathbf{u} \cap \mathbf{v}) \sqcup (\mathbf{u} \Delta \mathbf{v})$, where \sqcup denotes the disjoint union, the second equality leverages the

independence of $\{x_i\}$, the third equality uses the definition of expectation, and the last equality is based on the previous result $\mathbb{E}_{x_i} [\tilde{k}_i(x_i, x'_i)] = 0$. This finishes the proof.

Proof of Theorem 3. The conditional zero mean property and the conditional orthogonality in Theorem 2 imply that

$$\text{Cov} \left(\hat{f}_{\mathbf{u}|t}(\cdot, t), \hat{f}_{\mathbf{v}|t}(\cdot, t) \right) = \int \hat{f}_{\mathbf{u}|t}(\mathbf{x}_{\mathbf{u}}, t) \hat{f}_{\mathbf{v}|t}(\mathbf{x}_{\mathbf{v}}, t) dF(\mathbf{x}) = 0, \quad \forall \mathbf{u} \neq \mathbf{v}, \forall t. \quad (33)$$

(c) Local variance decomposition: We have

$$\begin{aligned} \mathbb{V}_{\mathbf{x}} \left(\hat{f}(\mathbf{x}, t) \right) &= \mathbb{V}_{\mathbf{x}} \left(\sum_{\mathbf{u} \subseteq \mathcal{D}} \hat{f}_{\mathbf{u}|t}(\mathbf{x}_{\mathbf{u}}, t) \right) \\ &= \sum_{\mathbf{u}, \mathbf{v} \subseteq \mathcal{D}} \text{Cov} \left(\hat{f}_{\mathbf{u}|t}(\cdot, t), \hat{f}_{\mathbf{v}|t}(\cdot, t) \right) \\ &= \sum_{\mathbf{u} \subseteq \mathcal{D}} \mathbb{V}_{\mathbf{x}} \left(\hat{f}_{\mathbf{u}|t}(\mathbf{x}_{\mathbf{u}}, t) \right) + \sum_{\mathbf{u} \neq \mathbf{v}} \text{Cov} \left(\hat{f}_{\mathbf{u}|t}(\cdot, t), \hat{f}_{\mathbf{v}|t}(\cdot, t) \right) \\ &= \sum_{\mathbf{u} \subseteq \mathcal{D}} \mathbb{V}_{\mathbf{x}} \left(\hat{f}_{\mathbf{u}|t}(\mathbf{x}_{\mathbf{u}}, t) \right), \end{aligned}$$

where the first equality follows from FOED, the second equality comes from the definition of variance as the sum of covariances between all pairs of effect functions, the third equality splits the total variance into individual variances and cross-effect covariances, and the last equality follows from the conditional orthogonality as shown in Eq. (33).

(d) Global variance decomposition: This result directly follows by taking the expectation with respect to the local variance decomposition, which finishes the proof.

Proof of Theorem 4. Utilizing the independence between the input variable \mathbf{x} and time

t , along with the conditional mean given by Theorem 2(b), we have

$$\begin{aligned}
V_{\mathbf{u}|t}(t) &= \mathbb{V}_{\mathbf{x}_{\mathbf{u}}} \left(\hat{f}_{\mathbf{u}|t}(\mathbf{x}_{\mathbf{u}}, t) \right) \\
&= \mathbb{V}_{\mathbf{x}_{\mathbf{u}}} \left(\left(\delta_t^2 \mathbf{k}_t \odot \left(\bigodot_{i \in \mathbf{u}} \delta_i^2 \mathbf{k}_i \right) \right)^\top \gamma \right) \\
&= \gamma^\top \mathbb{V}_{\mathbf{x}_{\mathbf{u}}} \left(\left(\delta_t^2 \mathbf{k}_t \odot \left(\bigodot_{i \in \mathbf{u}} \delta_i^2 \mathbf{k}_i \right) \right)^\top \right) \gamma \\
&= \gamma^\top (\delta_t^4 \mathbf{k}_t \mathbf{k}_t^\top) \odot \left(\bigodot_{i \in \mathbf{u}} \mathbb{V}_{x_i} (\delta_i^2 \mathbf{k}_i) \right) \gamma \\
&= \gamma^\top (\delta_t^4 \mathbf{k}_t \mathbf{k}_t^\top) \odot \left(\bigodot_{i \in \mathbf{u}} \delta_i^4 \mathbb{E}_{x_i} [\mathbf{k}_i \mathbf{k}_i^\top] \right) \gamma,
\end{aligned}$$

where the third equality uses the property $\mathbb{V}(\mathbf{X}\mathbf{B}) = \mathbf{B}^\top \mathbb{V}(\mathbf{X}) \mathbf{B}$, the forth equality leverages the independence between the input variable \mathbf{x} and time t and the property of Hadamard product, and the last equality follows from the identity $\mathbb{V}(\mathbf{X}) = \mathbb{E}[\mathbf{X}\mathbf{X}^\top] - \mathbb{E}[\mathbf{X}]\mathbb{E}[\mathbf{X}]^\top$ and the property $\mathbb{E}_{x_i} [\tilde{k}_i(x_i, x'_i)] = 0$. Taking the expectation of $V_{\mathbf{u}|t}(t)$ with respect to time t yields

$$\begin{aligned}
V_{\mathbf{u}} &= \mathbb{E}_t \left[\gamma^\top (\delta_t^4 \mathbf{k}_t \mathbf{k}_t^\top) \odot \bigodot_{i \in \mathbf{u}} \delta_i^4 \mathbb{E}_{x_i} [\mathbf{k}_i \mathbf{k}_i^\top] \gamma \right] \\
&= \gamma^\top \left(\delta_t^4 \mathbb{E}_t [\mathbf{k}_t \mathbf{k}_t^\top] \odot \left(\bigodot_{i \in \mathbf{u}} \delta_i^4 \mathbb{E}_{x_i} [\mathbf{k}_i \mathbf{k}_i^\top] \right) \right) \gamma,
\end{aligned}$$

which finishes the proof.